

Registration Number:

Registration Date:

The information on this cover page is based on the most recent submission data from the authors. It may vary from the final published article. Any fields remaining blank are not applicable for this manuscript.

1 **Struan Loughlin^{1,2}, Hannah M. Costello², Andrew J. Roe³, Charlotte Buckley⁴, Stuart M.**
2 **Wilson³, Matthew A. Bailey¹ and Morag K. Mansley^{1,2,3}**

3

4 MAPPING THE TRANSCRIPTOME UNDERPINNING ACUTE CORTICOSTEROID ACTION WITHIN
5 THE CORTICAL COLLECTING DUCT

6

7 Running title: Corticosteroid-induced transcriptome in the collecting duct

8

9 ¹Cellular Medicine Research Division, University of St Andrews, North Haugh, St Andrews, KY16 9TF, UK;
10 ²Centre for Cardiovascular Science, Queen's Medical Research Institute, The University of Edinburgh,
11 Edinburgh, EH16 4TJ, UK; ³Division of Pharmacy, School of Medicine, Pharmacy and Health, Durham
12 University Queen's Campus, Stockton-on-Tees, TS17 6BH, UK; ⁴Strathclyde Institute of Pharmacy and
13 Biomedical Sciences, University of Strathclyde, Glasgow, G4 0RE, UK.

14

15 *Address for Correspondence: Dr Morag K. Mansley, ¹Cellular Medicine Research Division, University of St
16 Andrews, North Haugh, St Andrews, KY16 9TF, UK. Email: mkm27@st-andrews.ac.uk

17 Highest academic degrees for each author: Loughlin - BSc; Costello - PhD; Roe - MSc; Buckley - PhD;
18 Wilson - DSc; Bailey - PhD; Mansley - PhD.

19

20

21

22

23

24 **Key Points**

- 25 • We report the transcriptomes associated with acute corticosteroid regulation of ENaC activity in
26 polarised mCCD_{cl1} collecting duct cells.
- 27 • 9 genes were regulated by aldosterone (ALDO), 0 with corticosterone alone and 151 with
28 corticosterone when 11 β HSD2 activity was inhibited.
- 29 • We validated 3 novel ALDO-induced genes: *Rasd1*, *Sult1d1* and *Gm43305* in primary cells isolated
30 from a novel principal cell reporter mouse.

31
32
33
34
35
36
37
38
39
40
41
42
43
44
45
46
47
48
49
50
51
52
53
54
55
56
57
58

59 **Abstract**

60

61 **Background**

62 Corticosteroids regulate distal nephron and collecting duct Na⁺ reabsorption, contributing to fluid-volume and
63 blood pressure homeostasis. The transcriptional landscape underpinning the acute stimulation of the epithelial
64 sodium channel (ENaC) by physiological concentrations of corticosteroids remains unclear.

65 **Methods**

66 Transcriptomic profiles underlying corticosteroid-stimulated ENaC activity in polarised mCCD_{cl1} cells were
67 generated by coupling electrophysiological measurements of amiloride-sensitive currents with RNAseq.
68 Generation of a principal cell-specific reporter mouse line, mT/mG-Aqp2Cre, enabled isolation of primary
69 collecting duct principal cells by FACS and ENaC activity was measured in cultured primary cells following
70 acute application of corticosteroids. Expression of target genes was assessed by qRT-PCR in cultured cells or
71 freshly isolated cells following acute elevation of steroid hormones in mT/mG-Aqp2Cre mice.

72 **Results**

73 Physiological relevance of the mCCD_{cl1} model was confirmed with aldosterone-specific stimulation of SGK1
74 and ENaC activity. Corticosterone only modulated these responses at supraphysiological concentrations or when
75 11βHSD2 was inhibited. When 11βHSD2 protection was intact, corticosterone caused no significant change in
76 transcripts. We identified a small number of aldosterone-induced transcripts associated with stimulated ENaC
77 activity in mCCD_{cl1} cells and a much larger number with corticosterone in the absence of 11βHSD2 activity.
78 Principal cells isolated from mT/mG-Aqp2Cre mice were validated and assessment of identified aldosterone-
79 induced genes revealed that *Sgk1*, *Zbtbt16*, *Sult1d1*, *Rasd1* and *Gm43305* are acutely upregulated by
80 corticosteroids both *in vitro* and *in vivo*.

81 **Conclusions**

82 This study reports the transcriptome of mCCD_{cl1} collecting duct cells and identifies a small number of
83 aldosterone-induced genes associated with acute stimulation of ENaC, including 3 previously undescribed
84 genes.

85

86

87

88

89

90

91 **Introduction**

92 Aldosterone (ALDO) and cortisol both influence blood pressure: ALDO as the final effector in the renin-
93 angiotensin-aldosterone system (RAAS), promoting Na⁺ reabsorption in the kidney; cortisol, in addition to
94 being thought of as a “stress” hormone, being linked to the circadian rhythm of blood pressure. Within the
95 kidney, ALDO acts specifically in the cells of the “aldosterone-sensitive distal nephron” (ASDN), where the
96 mineralocorticoid receptor (MR) and the enzyme 11-beta-hydroxysteroid dehydrogenase type 2 (11βHSD2) are
97 both expressed.¹ 11βHSD2 converts circulating cortisol to the inactive metabolite cortisone, conferring ALDO
98 specificity to the ASDN which has previously been demarked as the late distal convoluted tubule (DCT2),
99 connecting tubule (CNT) and collecting duct (CD).¹ There is now increasing evidence that 11βHSD2 is absent
100 in the DCT,^{2,3} thus the boundaries of the ASDN may need updating to include the CNT and CCD only. Genetic
101 mutations or pharmacological inhibition of 11βHSD2 cause hypertension in both humans⁴ and rodents,⁵
102 highlighting the importance of 11βHSD2 to blood pressure control. Additionally, recent evidence suggests that
103 in states of glucocorticoid excess (e.g. chronic stress, obesity), cortisol may cause hypertension due to aberrant
104 activation of renal sodium transport. Causal mechanisms are not fully understood but activation of the epithelial
105 sodium channel (ENaC) *via* MR and the glucocorticoid receptor (GR) have been implicated.⁶

106 The classical actions of corticosteroids in the kidney involve hormones binding cytosolic steroid receptors
107 within the epithelial cells lining the ASDN, modulating transcriptional processes and subsequent stimulation of
108 Na⁺ reabsorption.⁷ This involves the transepithelial movement of Na⁺ back to the circulation, firstly crossing the
109 apical membrane *via* the epithelial Na⁺ channel (ENaC) and subsequent extrusion across the basolateral
110 membrane *via* the Na⁺/K⁺ ATP-ase. ENaC is rate-limiting in this process and is subject to regulation by a
111 number of different hormones and bioactive factors.⁸ Elucidation of the transcriptional targets of corticosteroid
112 action in the kidney have involved many studies over the past two decades which have made use of a variety of
113 model systems e.g. whole kidney homogenate, microdissected tubules,⁹ primary cells isolated by FACS^{10, 11} as
114 well as a number of cell lines;¹²⁻¹⁴ utilising ever-improving technology e.g. SAGE analysis, microarrays and
115 more recently next generation sequencing. Key transcripts have been identified which encode target proteins
116 including the serum and glucocorticoid-induced kinase 1 (SGK1) and the glucocorticoid-induced leucine zipper
117 protein (GILZ), both of which have been shown to regulate ENaC activity.¹⁵⁻¹⁷ However, there are discrepancies
118 regarding the relative roles of these steroid-induced genes particularly considering the phenotypic difference in
119 mice following nephron-specific deletion of MR¹⁸ compared with deletion of e.g. SGK1¹⁹ or GILZ.²⁰
120 Furthermore, the high concentrations of corticosteroids used to identify relevant genes in various model systems
121 leaves the physiological relevance of these transcripts to steroid-induced ENaC activity within the distal
122 nephron unclear.

123 The objective of this study was therefore to apply an unbiased, reductionist approach to generate transcriptomic
124 profiles associated with the acute Na⁺ retaining effects of corticosteroids in a physiologically relevant murine
125 cell model of the cortical CD, mCCD_{cl1} cells. These display many of the reported features of Na⁺ absorbing
126 principal cells of the collecting duct: predominant amiloride-sensitive Na⁺ conductance *via* ENaC, a K⁺
127 conductance mediated *via* the renal outer medullary K⁺ channel (ROMK),²¹ functional 11βHSD2 activity,²² as
128 well as regulation of these transport pathways by physiological concentrations of hormones including

129 aldosterone and arginine vasopressin (AVP).^{22, 23} We report the full transcriptome of the mCCD_{cl1} cells and
130 identify 9 ALDO-induced genes. Lack of transcriptional effects of corticosterone (CORT) confirm 11 β HSD2
131 activity, and upon pharmacological inhibition of this enzyme, CORT modulated 151 genes. Identified ALDO-
132 induced genes were validated in mCCD_{cl1} cells and subsequently in primary CD cells isolated from a newly
133 generated mT/mG-Aqp2Cre reporter mouse. Identified ALDO-induced targets were subsequently measured in
134 both cultured primary principal cells treated with steroids or from principal cells isolated directly from reporter
135 mice following acute injection of corticosteroids. Our findings confirm both *Sgk1* and *Zbtb16* as acute ALDO-
136 induced genes, and we further report *Rasd1*, *Sult1d1* and the unannotated *Gm43305* which encodes a lncRNA.

137 **Methods**138 Culture of mCCD_{cl1} cells

139 mCCD_{cl1} cells (Prof. Bernard Rossier, University of Lausanne, Switzerland) were maintained in routine
 140 culture^{22, 24} at 37°C and 5% CO₂, in phenol-red free DMEM/F12 media supplemented with FBS (2%),
 141 triiodothyronine (1 nmol/l), sodium selenite (5 ng/ml), insulin (5 µg/ml), transferrin (5 µg/ml), L-glutamine (200
 142 mmol/l), penicillin (100 U/ml), streptomycin (100 µg/ml), dexamethasone (50 nmol/l) and EGF (10 ng/ml).
 143 Cells were used between passages 29-35. For experiments, cells were seeded onto 0.4 µm polyester filter
 144 membranes (Corning CoStar Snapwells) and grown for 9-11 days with media exchange every 2 days. 48 h
 145 before experimental protocols, media was replaced with DMEM/F12 media supplemented with charcoal-
 146 stripped media (2%), penicillin (100 U/ml) and streptomycin (100 µg/ml). For the final 24 h, media was
 147 replaced with DMEM/F12 with penicillin (100 U/ml) and streptomycin (100 µg/ml).

148 Quantification of transepithelial ion transport

149 Transepithelial voltage (V_{te}) and resistance (R_{te}) were measured using an epithelial volt-ohm-meter (EVOM)
 150 with chopstick “STX” electrodes (World Precision Instruments, Hertfordshire, UK). The equivalent short circuit
 151 current (I_{eq}) was subsequently calculated by Ohm’s Law. V_{te} is shown relative to an earth electrode in the
 152 basolateral bath,²⁵ therefore a negative I_{eq} reflects either apical to basolateral movement of cations, basolateral to
 153 apical movement of anions or some combination of the two. Amiloride (10 µM, 10 min) was applied to the
 154 apical bath to determine the ENaC-mediated proportion of I_{eq} .

155 RNA sequencing

156 Total RNA was extracted from cells using the Rneasy kit (Qiagen) following electrophysiological
 157 measurements. RNA was subject to quality control (RNA ScreenTape) and RIN values were ≥ 9.0 . TruSeq
 158 stranded mRNA-seq libraries were generated from each total RNA sample (24 libraries in total). Libraries were
 159 sequenced using the Illumina HiSeq 4000 Platform with 150 base pair paired-end reads. Reads were trimmed for
 160 quality (Cutadapt version 1.121) at the 3’ end using a threshold of Q30 and for adapter sequences of the TruSeq
 161 stranded mRNA kit (AGATCGGAAGAGC) using Cutadapt version 1.121.²⁶ Reads after trimming were
 162 required to have a minimum length of 50. The raw RNAseq data have been uploaded to the Sequence Read
 163 Archive at NCBI, with the project ID: PRJNA820455. The reference used for mapping was the *Mus musculus*
 164 genome from Ensembl, assembly GRCm38, annotation version 84. Reads were aligned to the reference genome
 165 using STAR2 version 2.5.2b.²⁷ The raw counts table was filtered to remove rows consisting of predominantly
 166 near-zero counts (values had to be >0.05 across 5 samples), filtering on counts per million (CPM) to avoid
 167 artefacts due to library depth. Initial exploratory analysis indicated an outlier in the dataset, which was removed
 168 and subsequent filtering and normalisation performed again for downstream analysis. Following filtering,
 169 17,962 genes remained. Differential analysis was carried out with EdgeR²⁸ (version 3.16.5) and compared all
 170 possible combinations from the 4 experimental conditions.

171 Generation of a principal cell-specific reporter mouse

172 Aqp2Cre mice²⁹ (The Jackson Laboratory, USA) were crossed with mT/mG (tdTomato-GFP) mice³⁰ (Prof. Neil
 173 Henderson, The University of Edinburgh, UK). Both mouse strains were on a C57BL/6 background. To ensure
 174 kidney-specific Cre expression, female AQP2-Cre mice were bred with male mT/mG mice; female offspring
 175 which were heterozygous for both AQP2-Cre and mT/mG were subsequently bred with male mice homozygous
 176 for mT/mG. Genotyping for AQP2-Cre was carried out using a forward primer 5'-
 177 CTCTGCAGGAAGTGGTGCTGG-3' and reverse primer 5'-GCGAACATCTTCAGGTTCTGCGG-3'.
 178 Genotyping for mT/mG was carried out using the forward primer 5'-CTCTGCTGCCTCCTGGCTTCT-3' and
 179 reverse primers: wildtype 5-CGAGGCGGATCACAAGCAATA-3' and mutant 5'-
 180 TCAATGGGCGGGGTCGTT-3'. Experiments were performed on male mice aged 10-30 weeks, under the
 181 authority of a UK Home Office Project License and following approval by the University's Animal Welfare and
 182 Ethical Review Board.

183 Isolation and culture of primary principal cells

184 Mice (wild-type, mT/mG^{+/+}-Aqp2Cre^{-/-} and mT/mG^{+/+}-Aqp2Cre^{+/-}) were terminated by rising CO₂ and PBS
 185 injected into the left ventricle to remove blood. Kidneys were excised, decapsulated and stored in ice-cold PBS.
 186 Both kidneys were manually chopped into small pieces and then homogenised in gentleMACS™ C Tubes
 187 (Miltenyi Biotec, Surrey, UK).³¹ Digestion buffer contained: RPMI supplemented with Collagenase V
 188 (0.425 mg/ml), Collagenase D (0.625 mg/ml), Dispase II (1 mg/ml), DNase I (30 µg/ml), penicillin (100 U/ml)
 189 and streptomycin (100 µg/ml). Cellular suspensions were digested for 30 min at 37°C before a second
 190 dissociation in the gentleMACS™ Dissociator. An equal volume of neutralisation buffer (PBS supplemented
 191 with FBS 2% vol/vol and EDTA 1 µM) was added and cell suspensions were passed sequentially through
 192 100 µm, 70 µm and 40 µm cell strainers. Cells were pelleted by centrifugation and red cell lysis was carried out
 193 using red blood cell lysis buffer (Sigma, Dorset, UK). Cells were pelleted and resuspended in 1 ml neutralisation
 194 buffer.

195 Cells were analysed and sorted using either a BD FACS Aria II or BD FACS Aria Fusion cell sorter. 405 nm,
 196 488 nm and 561 nm lasers were used for excitation of DAPI, GFP and tdTom, respectively. Wild-type C57BL/6
 197 and mT/mG^{+/+}-Aqp2Cre^{-/-} kidney samples were processed first to define gates before processing
 198 mT/mG^{+/+}-Aqp2Cre^{+/-} samples. DAPI, at a final concentration of 0.1 µg/ml, was added to cells immediately
 199 prior to sorting. Cells were gated for a stable recording, singlets (plotting forward scatter area vs. height), cells
 200 (forward scatter area vs. side scatter area), live cells (DAPI vs. forward scatter area), followed by exclusive gates
 201 for both tdTom and GFP (Supplementary Figure 3). From the GFP gate, a further gate was added to remove
 202 autofluorescence events detected within that channel and a final gate to remove a mixed population of both
 203 tdTom and GFP. Cell sorting was performed with a 100 µm nozzle and due to the starting cell numbers and the
 204 relatively small percentage of GFP positive events, a yield sort followed by a purity sort was employed to
 205 optimise sort/time efficiency. For initial validation studies, 100,000 tdTom cells were collected and all possible
 206 GFP cells. Once the GFP population was validated, only GFP events were collected. Flow cytometry data was
 207 analysed using FCS Express 7 (De Novo Software, Pasadena, CA, USA).

208 For downstream experiments, GFP⁺ sorted cells were then either spun down, supernatant removed and RLTPlus
 209 buffer added for RNA extraction or instead were directly plated onto gelatin-coated 12 well plates with
 210 complete media. Cells were maintained under identical conditions as those used for culture of mCCD_{cl1} cells
 211 with the addition of gelatin coating of either the initial 12 well plate or the permeable membrane used for
 212 growing polarised monolayers.

213 Acute steroid treatment of mT/mG-Aqp2Cre mice

214 Male mT/mG^{+/+}-Aqp2Cre^{+/-} mice, aged 10-30 weeks, were administered carbenoxolone (CBX) at 2.5mg/kg
 215 BW/day *po* (in drinking water) to inhibit endogenous 11 β HSD2,³² control animals were given *ad lib* access to
 216 drinking water for 8 days. Animals were weighed every morning (between 08:00-10:00) 5 days prior to
 217 CBX/control treatment and subsequently throughout. On day 9 at 08:30, mice were administered with a single
 218 dose of steroid: aldosterone (10 μ g/kg BW),³³ corticosterone (CORT, 0.5 mg/kg BW) or solvent vehicle
 219 (5 % EtOH) *via ip* injection. After 3 h, mice were sacrificed by rising concentration of CO₂ and CD cells
 220 (GFP⁺) were then isolated by FACS.

221 Immunofluorescence imaging

222 Kidneys were decapsulated, bisected (left kidney: longitudinal section and right kidney: transverse section) and
 223 immersed in MeOH-free 4% PFA for 2 h at 4°C. Half kidneys were then washed twice with PBS, transferred to
 224 an 18% sucrose solution at 4°C overnight and then embedded in OCT, frozen and sectioned at 10 μ m onto glass
 225 slides. Sections were permeabilised with 0.2% Triton X-100 for 10 min, blocked with 10% donkey serum for
 226 1 h and subsequently washed with TBS-T (0.05% Tween 20). Sections were mounted in ProLong Diamond
 227 Antifade Mountant (Life Technologies, Paisley, UK) and imaged at 40X using a Zeiss AxioScan.Z1.

228 All images were processed using Fiji,³⁴ and the same process was applied to images from both mT/mG^{+/+}-
 229 Aqp2Cre^{-/-} and mT/mG^{+/+}- Aqp2Cre^{+/-} kidneys. Channels were split and a background subtraction (50 pixels)
 230 was performed on the 555 nm channel. For low magnification images, the 488 nm channel image was duplicated
 231 and a Gaussian blur (sigma = 10) applied. To separate the Cre-GFP signal from the tubule-generated
 232 autofluorescence, the blurred image was subtracted from the raw image and a threshold applied such that on the
 233 Cre-GFP remained (~0.04 %). This was used to generate a mask, which was changed to 16-bit and a Gaussian
 234 blur (sigma = 7) applied. This was used as the green channel, and the autofluorescence as the grey channel. For
 235 high magnification images, the 488 nm channel image was duplicated and a Gaussian blur (sigma = 3) applied.
 236 The blurred image was again subtracted from the raw image and a threshold applied such that on the Cre-GFP
 237 remained (~0.01%). This was used to generate a mask, which was changed to 16-bit and a Gaussian blur (sigma
 238 = 2) applied and used as the green channel.

239 qRT-PCR

240 Total RNA was extracted from cells, either grown as monolayers in culture on filter membranes or directly
 241 following FACS of CD cells, using a QIAGEN RNeasy Plus Micro Kit. The integrity of the RNA preparations
 242 was verified using the Agilent RNA 6000 Pico Kit and Agilent 2100 Bioanalyser, samples with RIN values <7.5
 243 were excluded. cDNA was transcribed from total RNA using Applied Biosystems High Capacity cDNA Reverse

244 Transcription Kit (Life Technologies). For experiments using lysates from cells grown in culture, 500 ng RNA
245 was used and cDNA was diluted 1:20 to correlate to the middle of the 7-point calibration curve generated from
246 serial dilutions. For experiments using isolated primary CD cells from mT/mG-AQP2Cre mice, 1 ng RNA was
247 used, as determined by the lowest yield across the samples. cDNA was diluted 1:10, also to correlate with the
248 middle of the calibration curve. qRT-PCR was performed using a Roche Light-Cycler 480 II using a probe-
249 based assay (Roche Universal Probe Library, Sigma, Dorset, UK). Primers were designed using the ProbeFinder
250 software within the Roche Assay Design Centre. Samples were run in triplicate and only Cq values with a
251 standard deviation >0.3 were excluded. A selection of reference genes (*Actb1*, *HPRT*, *Tbp* and *18S*) were tested
252 and included if expression remained unaltered across all samples (Supplementary Figures 2, 4 and 5). Negative
253 controls included reverse transcriptase negative, RNA negative and H₂O only.

254 Western analysis

255 Cells were washed with ice-cold PBS (x3), lysed in lysis buffer²⁵ and vortexed. Protein concentration was
256 quantified by Bradford assay (BioRad, Hertfordshire, UK). Samples were prepared by adding a fixed mass of
257 protein lysate to sample buffer, reducing and denaturing by heating at 95°C for 5 min in the presence of 2-
258 mercaptoethanol. Samples were subsequently fractionated on 10% SDS polyacrylamide gels, transferred to
259 PVDF membranes, blocked and probed with primary antibodies of interest and respective HRP-linked
260 secondary antibodies. Primary antibodies against Thr^{346/356/366}-phosphorylated and total forms of the protein
261 encoded by n-myc downstream regulated 1 (NDRG1), as well as total serum and glucocorticoid-regulated
262 kinase 1 (SGK1) were purchased from the Dundee Protein Phosphorylation Unit, University of Dundee
263 (Dundee, UK). The antibody against β-actin was from Sigma (Dorset, UK). Immunoreactive proteins were
264 visualised by enhanced chemi-luminescence and quantified by densitometric measurements, as described
265 previously.³⁵

266 Data analysis

267 Data are expressed as mean±95% CI. For western blotting and qRT-PCR, due to uneven distribution of data
268 expressed as fold-change, all data were log-transformed. All datasets were subject to normality testing (Shapiro-
269 Wilks) followed by either parametric testing: unpaired t-test, one-way or two-way ANOVA or non-parametric
270 testing: Mann-Whitney or Kruskal-Wallis, where appropriate. Post-hoc analysis was also carried out where
271 appropriate, details of specific tests used are included in the figure legends.

272 **Results**

273 **Modulation of ENaC and SGK1 activity by corticosteroids in mCCD_{cl1} cells.** Polarised mCCD_{cl1} cells
 274 generated an average transepithelial voltage (V_{te}) of 22.8 ± 11.3 mV and resistance R_{te} of 1.6 ± 0.6 $k\Omega \cdot cm^2$, giving
 275 an average equivalent short-circuit current (I_{eq}) of 13.7 ± 3.4 $\mu A \cdot cm^{-2}$ ($n=144$). I_{eq} reflects ENaC-mediated Na^+
 276 transport as $\sim 95\%$ is inhibited by amiloride ($10 \mu M$).²⁴ Corticosterone (CORT) stimulated the amiloride-
 277 sensitive current (I_{ami-3h}) at concentrations ≥ 100 nM, consistent with endogenous activity of the “protective”
 278 11β HSD2 (Figure 1Ai). Inhibiting 11β HSD2 with carbenoxolone (CBX, $10 \mu M$, 30 min) revealed a
 279 concentration-dependent stimulation of ENaC-mediated Na^+ transport by CORT at concentrations ≥ 1 nM
 280 (Figure 1Ai). Baseline current was not altered in cells treated with CBX alone. Aldosterone (ALDO) also
 281 stimulated I_{ami} in a concentration-dependent manner; this was independent of CBX pre-treatment, consistent
 282 with ALDO not being a substrate for this enzyme (Figure 1Bi). CORT-induced Na^+ transport correlated with
 283 increased activity and expression of the protein serum and glucocorticoid induced kinase 1 (SGK1), Figure 1Aii
 284 and iii. SGK1 abundance under basal conditions is very low,³⁶ however there is clear activity of this kinase as
 285 per the basal levels of phosphorylation of specific residues in a downstream target NDRG1. Both SGK1 activity
 286 and expression were increased with ALDO (Figure 1Bii and iii).

287 **Mapping the transcriptomes associated with acute corticosteroid stimulation of ENaC-mediated Na^+**
 288 **transport.** Polarised mCCD_{cl1} cells were treated for 3 h with either solvent vehicle, ALDO (3 nM) or CORT
 289 (100 nM), the latter in the absence or presence of CBX ($10 \mu M$). Consistent with the concentration response
 290 assays ALDO, or CORT in the presence of CBX, stimulated I_{ami} compared to control whilst CORT in the
 291 absence of CBX did not alter I_{ami} (Figure 2A). cDNA libraries were generated across each of the 4 groups ($n=6$)
 292 which underwent 150 bp paired-end sequencing. Over 94% of trimmed reads were mapped to the genome and
 293 of those, 97.0–98.4% mapped as pairs.

294 Differential gene expression analysis compared all possible contrasts of experimental condition using thresholds
 295 of a minimum \log_2 fold change of 1 and a false discovery rate < 0.05 (Table 1). Volcano plots were generated
 296 and show the differential expression of genes in cells treated with vehicle compared to ALDO, CORT or
 297 CBX+CORT (Figure 2B). 9 genes were identified in the ALDO group compared to the control group and 151
 298 genes were differentially expressed in the CBX+CORT group compared to the control group (Figure 2B). Table
 299 2 lists all transcripts regulated by ALDO and Table 3 lists the top 15 upregulated and all downregulated
 300 annotated genes in the CBX+CORT group. No transcripts were differentially expressed in the CORT group and
 301 this finding correlates with a lack of stimulated I_{ami} . All 9 transcripts differentially expressed in the ALDO *vs.*
 302 control group were also differentially expressed in the CBX+CORT group *vs.* control. The complete list of
 303 differentially regulated genes, as well as a counts table across the 4 experimental groups can be found in the
 304 supplementary excel file. Five of the genes identified (*Sgk1*, *Sult1d1*, *Gm43305*, *Rasd1* and *Zbtb16*) were
 305 subsequently validated by qRT-PCR in polarised mCCD_{cl1} cells (Supplementary Figure S1). Cells were treated
 306 in similar manner: CORT (100 nM) or vehicle for 3 h, following pre-incubation with CBX ($10 \mu M$) or vehicle
 307 for 30 min, or treated with ALDO (3 nM) or vehicle for 3 h. Electrophysiological measurements to monitor
 308 ENaC activity were made prior to RNA extraction (data not shown).

309 **Generation and validation of a principal cell-specific reporter mouse.** The mT/mG mouse line,³⁰ which
 310 ubiquitously express tdTomato (tdTom) in cell membranes (mT) or upon Cre excision express enhanced GFP
 311 (mG), was crossed with the Aqp2Cre line.²⁹ Fixed longitudinal sections of kidneys from adult offspring were
 312 imaged for tdTom and GFP labelling. mT/mG positive and Aqp2Cre null mice e.g. mT/mG^{+/+}-Aqp2Cre^{-/-},
 313 demonstrated membrane labelling of tdTom in both cortex and medullary regions (Figure 3Ai). Distinct
 314 differences in labelling can be seen in the cortex where brush border membranes of the proximal tubules exhibit
 315 less evenly distributed membrane-associated markers than distal tubules and collecting ducts (Figure 3Aii). This
 316 is consistent with the expression pattern previously reported in kidney tissue.²⁹ Negligible eGFP labelling was
 317 detected (Figure 3Aiii). Kidney sections from adult mice homozygous for mT/mG and hemizygous for
 318 Aqp2Cre, e.g. mT/mG^{+/+}-Aqp2Cre^{+/-} mice (B), displayed both tdTom and Cre-induced eGFP labelling in the
 319 cortex and medulla (Figure 3Bi-iii). The eGFP labelling of tubules is low, possibly indicating low
 320 recombination efficiency of the Aqp2Cre line, in our hands.

321 Expression of nephron segment-specific markers were determined in tdTom and GFP+ populations (Table 4).
 322 Whilst the tdTom population was enriched for markers consistent with the proximal tubule (NHE3) and the loop
 323 of Henle (NKCC2), the GFP+ population was enriched for markers of the CD. In particular, principal cell
 324 markers ROMK, α -ENaC and 11 β HSD2, but also β -intercalated cell markers V-ATPase β 1 and pendrin, but not
 325 the α -intercalated cell marker AE1 (Table 4). NCC expression was detected in both populations.

326 To determine functional properties, one isolated population was grown in culture over several weeks. Cells were
 327 subsequently seeded onto permeable inserts; after 9-11 days baseline V_{te} and R_{te} were -20.3 ± 3.1 mV and
 328 5.1 ± 0.1 k Ω ·cm² respectively, giving rise to an I_{eq} of -3.9 ± 0.6 μ A·cm⁻² (values are mean \pm 95% CI, $n=25$). It was
 329 noted that over numerous passages V_{te} reduced, R_{te} increased, thus I_{eq} decreased (data not shown). Cells were
 330 therefore used between passages 4-8 for all experiments. Similar to the mCCD_{cl1} cells, application of amiloride
 331 (10 μ M, 10 min) inhibited basal I_{eq} to negligible values (Figure 5A), indicating a predominant amiloride-
 332 sensitive current in the primary principal cells. A concentration response assay to CORT \pm CBX revealed that
 333 CORT stimulated I_{ami-3h} at concentrations >100 nM and pre-incubating primary principal cells with CBX
 334 (10 μ M, 30 min) unveiled a concentration-dependent stimulation of I_{ami-3h} (Figure 4Ai). Stimulation of ENaC-
 335 mediated Na⁺ transport correlated with increased activity of SGK1 activity, as determined by phosphorylation of
 336 NDRG1-Thr^{346/356/366} (Figure 4Aii).

337 **Corticosteroid regulation of ENaC activity and identified ALDO-induced genes in cultured primary**
 338 **principal cells.** Primary principal cells were treated (3 h) with: CORT (10 nM) in the absence/presence of CBX
 339 (10 μ M, 30 min pre-incubation), ALDO (3 nM) or dexamethasone (DEX, 100 nM). Consistent with the
 340 concentration response assays, CORT only stimulated I_{ami-3h} when cells were pre-incubated with CBX: 2.4 ± 0.3
 341 fold vs. without CBX: 1.2 ± 0.2 fold (Figure 5A, $n=8$). Both ALDO and DEX stimulated I_{ami-3h} by 2.0 ± 0.3 fold
 342 (Figure 5B, $n=8$) and $3.6 \pm$ fold (Fig 5C, $n=8$), respectively. Of the 8 targets tested: *Sgk1*, *Sult1d1*, *Gm43305*,
 343 *Rasd1*, *Zbtb16*, *Defb1*, *Gm16178* and *Gm9694*, expression of three were upregulated by CBX+CORT (10 nM) –
 344 *Sgk1*, *Gm43305* and *Zbtb16*. No targets were altered either by CORT or CBX alone (Figure 6). In cells treated
 345 with ALDO, expression of 3 out of 8 target transcripts tested was increased: *Sgk1*, *Rasd1* and *Zbtb16* (Figure
 346 7A). Finally, in cells treated with DEX, all but one target tested (*Gm9694*) was upregulated (Figure 7B).

347 **Corticosteroid regulation of identified ALDO-induced genes in principal cells isolated from mT/mG-**
 348 **Aqp2Cre mice.** We measured expression of 6 ALDO-induced targets: *Sgk1*, *Sult1d1*, *Gm43305*, *Rasd1*,
 349 *Zbtb16*, and *Defb1* in isolated primary principal cells following acute treatment with steroid hormones or
 350 respective controls. Of these, 4 were upregulated in mice treated with ALDO: *Sult1d1*, *Gm43305*, *Rasd1*,
 351 *Zbtb16* (Figure 8A). These 4 transcripts were also upregulated in mice treated with CBX+CORT. Notably
 352 *Sult1d1*, *Gm43305* and *Zbtb16* were also upregulated in the CORT group but also in the CBX group.

353

354 **Discussion**

355 We have mapped the transcriptomes underlying corticosteroid-regulated ENaC activity, identifying a small
 356 number of ALDO-regulated genes and larger number of CORT-regulated genes, the latter only when 11 β HSD2
 357 was inhibited. We utilised mouse mCCD_{cl1} cells,²² a well-described model of ASDN to couple transcriptomic
 358 with electrophysiological analysis. ENaC activity was stimulated by low nanomolar concentrations of ALDO²²,
 359 ³⁷ and by CORT at concentrations greater than 100 nM or when endogenous 11 β HSD2 activity was inhibited by
 360 CBX. The “gatekeeping” activity of this enzyme extends to complete absence of transcriptional activity by
 361 CORT. Isolation of primary principal cells from a novel reporter mouse enabled assessment of steroid-induced
 362 ion transport and target gene expression, the latter both *in vitro* and *in vivo*.

363 Deep sequencing of polarised mCCD_{cl1} cells revealed expression of genes associated with principal cells of
 364 CCD including: *Aqp2* (AQP2), *Hsd11b2* (11 β -HSD2), *Kcnj1* (ROMK), *Kcnj10* (Kir4.1), *Nr3c1* (GR), *Nr3c2*
 365 (MR), *Scnn1a* (α -ENaC), *Scnn1b* (β -ENaC), *Scnn1g* (γ -ENaC). With low expression of *Slc12a3* (NCC) and
 366 absence of *Pvalb* (parvalbumin), *Slc12a1* (NKCC2) and *Slc9a3* (NHE3), these cells likely represent epithelia
 367 from DCT2 onwards. Whilst there is low expression of *Atp6v1b1* (V-ATPase β 1), there is no detectable
 368 expression of either *Slc4a1* (AE1) or *Slc26a4* (pendrin), thus it seems mCCD_{cl1} cells reflect a principal cell
 369 population. This expression profile aligns with principal cell populations identified by scSeq of mouse kidney.³⁸
 370 ³⁹ Transcriptomic profiling of the related cell line, mpkCCD_{cl4},⁴⁰ revealed a similar pattern of transcripts, with
 371 the exception of *Kcnj1*, *Kcnj10* and *Nr3c2*.⁴¹ More recently, RNAseq analysis of a subclone of these cells,
 372 mpkCCD_{cl1}, whilst also having a similar pattern of transcripts, revealed low expression of *Nr3c2*, but *Kcnj1*,
 373 *Kcnj10*, *Kcnj16* and *Scnn1b* were absent.⁴² Functionally the mpkCCD_{cl4} cell line does not exhibit ALDO-
 374 sensitivity, requiring micromolar concentrations to exert a stimulatory effect on ENaC,^{40, 43, 44} consistent with the
 375 lack of, or very low abundance of, the MR.

376 We confirm both *Sgk1* and *Zbtb16* as early ALDO-induced genes,^{16, 33, 45, 46} and further identify *Rasd1*, *Sult1d1*
377 and an unannotated transcript *Gm43305*. SGK1 is well described as a steroid-induced protein which prevents
378 ubiquitin-mediated removal of ENaC in the apical membrane through phosphorylation of the ubiquitin-ligase
379 Nedd4-2.⁴⁷ *Zbtb16*, the promyelocytic leukaemia zinc finger protein (PLZF), was identified as an early ALDO-
380 induced gene in M1 cells expressing rat MR.⁴⁶ Overexpression of PLZF reduced basal I_{SC} but did not alter
381 dexamethasone-induced I_{SC} , suggesting that rather than mediating the stimulatory response of ALDO, PLZF
382 may negatively regulate ENaC in the CD.⁴⁶ Whilst *Rasd1* has not been directly linked to corticosteroid effects in
383 the CD, it has previously been identified as a downregulated transcript in SAGE analysis of the outer medullary
384 collecting duct (OMCD) in mice following 3 days of K^+ depletion.⁴⁸ *Rasd1* has been identified as an intercalated
385 cell-enriched transcript in mice.⁴⁹ Due to the potential plasticity of CD cells, or the de-differentiation of isolated
386 cells, it will be prudent to determine in which cell-type *Rasd1* is expressed *in vivo* and whether its induction by
387 ALDO relates to ENaC stimulation. It is of note that a related gene from the Ras superfamily: *Kras* (also known
388 as *KRas2a*) was previously identified as a steroid-induced transcript in amphibian A6 cells⁵⁰ and when co-
389 expressed with ENaC in oocytes, stimulated amiloride-sensitive currents.⁵¹ Whilst our data show expression of
390 *Kras*, we did not detect significant changes in expression with any steroid treatment tested. *Sult1d1* was also
391 upregulated by ALDO and two other family members *Sult1a1* and *Sult1b1* were upregulated in cells treated with
392 CBX+CORT. Sulfonation has been associated with inactivation of molecules to facilitate excretion,⁵² and it
393 may also regulate intracellular bioavailability.⁵³ SULT1D1 has been associated with catecholamine sulfation in
394 mouse kidney, thought to enhance excretion.⁵⁴ However, with no human orthologue of *Sult1d1*, it may represent
395 a species-dependent regulation of catecholamines. Finally, *Gm43305* is an unannotated transcript encoding a
396 long non-coding RNA located upstream of the olfactory receptor *Olfr49* on chromosome 14. Whether this
397 ALDO-induced lncRNA relates to the stimulation of ENaC remains unknown, but it is of interest whether
398 lncRNAs may be identified as yet another layer of regulation of ion transport processes in the distal nephron.

399 We compared acute ALDO-induced transcriptional events from this study with two recent studies which
400 mapped the transcriptomes of isolated primary cells of the ASDN following chronic ALDO treatment.^{10, 11} In
401 these 2 studies, mice kept on a low Na^+ diet for 5 days or infused with exogenous ALDO by osmotic minipump
402 for 6 days, had plasma [ALDO] of ~ 1.5 nM, which is comparable to the 3 nM used in our own study. Of the
403 ALDO-induced genes identified in the present study, both *Sult1d1* and/or *Sgk1* were identified as aldosterone-
404 regulated.^{10, 11} From the full transcriptome of the DCT/CNT/iCCD under control conditions,¹⁰ expression of 7
405 out of 9 of our ALDO-induced transcripts were detected, with the absence of 2 identified unannotated genes
406 *Gm43305* and *Gm9694*. The differences in ALDO-induced genes between our study and these others may
407 reflect the acute time-frame in which we measured transcriptional changes and may align with the concept of
408 early vs. late effects of ALDO in the ASDN.⁵⁵

409 ENaC-mediated Na⁺ transport in the ASDN is not normally responsive to CORT due to 11 β HSD2 activity.^{56, 57}
410 We confirmed ENaC cannot be stimulated by CORT at physiological concentrations in mCCD_{el1} cells²² and
411 subsequently demonstrated SGK1 expression/activity is also protected. Our transcriptomic data reveal that
412 11 β HSD2, in fact, fully abolishes the transcriptional effects of CORT and since no 11 β HSD1 expression was
413 detected, CORT is fully inactivated and cannot be re-activated in principal cells. Recent work suggests that the
414 ASDN may in fact not include the late DCT/early CNT, where basal ENaC activity is much greater than in the
415 CNT/CCD.⁵⁸ Dietary manoeuvres which raise plasma [ALDO] produce different effects on ENaC depending on
416 its location. Whilst ENaC activity is stimulated in both the DCT/CNT and CNT/CCD in mice maintained on a
417 high K⁺ diet,⁵⁹ ENaC activity is only stimulated in the CNT/CCD in mice maintained on a low Na⁺ diet.⁶⁰ The
418 MR, appears critical in both regions for steroid-induced ENaC activity as deletion abolishes these responses.^{59, 61}
419 It is interesting to speculate whether expression of the cellular machinery underpinning ALDO sensitivity differs
420 in these locations giving rise to different basal, as well as ALDO-induced, ENaC activity. There are mixed
421 reports regarding immunolocalization of 11 β HSD2 in the DCT^{2, 3, 62} and recent scSeq of murine kidneys report
422 low/negligible expression.^{38, 39, 63} We determined the transcriptomic effects of CORT in the absence of
423 11 β HSD2: ENaC activity was robustly stimulated and differential gene expression analysis revealed modulation
424 of a much larger number of genes compared to ALDO, including previously described steroid-induced targets:
425 GILZ, α -ENaC, and Per1.^{12, 13} All genes identified following ALDO treatment were identified in cells treated
426 with CBX+CORT, indicating a shared pathway of these hormones downstream of binding endogenous
427 receptors. The relative roles that the MR, GR or indeed both within the distal nephron, particularly where
428 11 β HSD2 is absent *vs.* present remains incompletely understood and warrants further investigation.

429 Generating mT/mG-Aqp2Cre mice to isolate primary CD cells is a similar strategy to previous studies that
430 utilised a TRPV5-eGFP reporter line to isolate primary CNT/CD cells¹⁰ or CD-specific cell isolation from wild-
431 type mice using either DBA lectin⁶⁴ or an L1-CAM antibody.¹¹ In our study, the isolated GFP+ cells were, as
432 expected, strongly enriched for genes characteristic of principal cells (encoding 11 β HSD2, ROMK, α -ENaC).
433 These cells also expressed genes encoding pendrin and AE1, associated with intercalated cells, albeit at a low
434 abundance. This finding is consistent with groups who isolated primary CD cells¹¹ or DCT2/CNT/initial CCD
435 cells.¹⁰ We do not think our results reflect non-specificity of Cre-recombinase as Aqp2Cre is not expressed in
436 intercalated cells.²⁹ Nor do we consider this to be contamination during isolation e.g. due to autofluorescence:
437 our gating strategy was stringent and we did not detect enrichment of markers associated with proximal tubule
438 cells, which exhibit strong autofluorescence. It is possible that either the isolated primary principal cells de-
439 differentiate rapidly or perhaps more likely, our results support the evidence that CD epithelia exhibit
440 plasticity.^{38, 65, 66} Indeed, scSeq analysis of murine kidney³⁸ reported a “transitional cell” type where high
441 expression of these IC transcripts were detected, at a similar level as *Aqp2*. The finding that the GFP+ cells
442 contain transcripts associated with PCs but also ICs is consistent with this. Importantly, functional assessment of
443 the isolated GFP+ cells revealed 11 β HSD2 activity as well as predominant amiloride-sensitive currents which
444 could be stimulated by aldosterone, therefore the isolated GFP+ cells phenotypically behave as Na⁺ absorbing
445 principal cells.

446 Primary principal cells grown on permeable supports in culture developed V_t and R_t in a manner analogous to
447 mCCD_{cl1} cells. R_t , of note, was much larger in these cells at $\sim 5 \text{ k}\Omega \cdot \text{cm}^2$, with a V_t of $\sim -20 \text{ mV}$ giving rise to an
448 I_{eq} of $\sim -3.5 \mu\text{A} \cdot \text{cm}^{-2}$. These currents are smaller than those recorded from mCCD_{cl1},^{22, 24} mpkCCD_{cl4},^{35, 40} as
449 well as primary CD cells isolated by DBA lectin,⁶⁴ but were almost completely abolished by amiloride
450 indicating a Na^+ absorbing phenotype *via* ENaC. Primary principal cells exhibited 11 β HSD2 activity and ENaC-
451 mediated currents were significantly stimulated by ALDO, CBX+CORT, as well as dexamethasone (DEX). This
452 correlates with currents measured in mCCD_{cl1} cells, confirming these cells represent a relevant model of
453 principal cells with the advantage that they do not de-differentiate over a small number of passages. Analysis of
454 identified ALDO-induced genes in primary cells grown in culture revealed ALDO and CBX+CORT both
455 upregulated *Sgk1*, *Rasd1* and *Zbtb16*, but ALDO also upregulated *Sult1d1* whereas CORT also upregulated
456 *Gm43305*. Interestingly, DEX upregulated 7 of 8 ALDO-induced genes tested. Studies have shown that whilst
457 DEX is considered a synthetic glucocorticoid, it can bind the MR as well as the GR.⁶⁷ In the transcriptomic data
458 from the mCCD_{cl1} cells, MR is expressed at 4x greater levels than GR, smaller than the 7x difference reported in
459 the mpkCCD_{cl1} cells,⁴² but similar to the 3x greater levels reported in the CD principal cell population identified
460 in scSeq analysis of murine kidney.³⁸

461 Building on our *in vitro* experiments, principal cell-specific reporter mice were acutely administered ALDO or
462 CORT \pm CBX.⁶⁸ Four of the identified ALDO-induced genes were upregulated in mice treated with either ALDO
463 or CBX+CORT: *Sult1d1*, *Gm43305*, *Rasd1* and *Zbtb16*. We noted that CBX treatment alone resulted in an
464 upregulation in expression of the ALDO-induced genes *Zbtb16*, *Gm43305* and *Sult1d1*. We did not, however,
465 detect changes in *Sgk1* across any of the groups. *Sgk1* has previously been shown to be upregulated in
466 microdissected CNT/CCD following 1 h ALDO treatment³³ and it is possible these rapid activation events were
467 complete by our 3 h collection point. However, from the data, it is clear that four of our identified
468 corticosteroid-induced genes remained upregulated after 3 h.

469 In summary, we report the transcriptional landscape associated with acute corticosteroid-induced ENaC activity
470 in principal cells of the CD. In addition to the previously described ALDO-induced targets *Sgk1* and *Zbtb16*, we
471 identify 3 additional acutely upregulated targets *Rasd1*, *Sult1d1* and the unannotated *Gm43305*. The potential
472 role that these genes play in mediating ALDO- induced ENaC activity in principal cells of the CD is of interest
473 and remains to be determined.

474

475

476

477

478

479

480

481 **Disclosures**

482 None.

483 **Funding**

484 This was work supported by Kidney Research UK: a Postdoctoral Fellowship PDF_008_20151127 and
485 Innovation Grant IN_001_20170302; the British Heart Foundation: Research Excellence Award RE/13/3/30183;
486 The Scottish Funding Council: St Andrews Research Funding Scheme; and the Society for Endocrinology:
487 Early Career Grant.

488 **Acknowledgements**

489 The authors are grateful to Dr. Laura Denby and Carolynn Cairns within the Centre for Cardiovascular Science
490 for giving guidance in preparing kidney homogenates for FACS. We thank Prof. Neil Henderson at The
491 University of Edinburgh for access to the mT/mG reporter mouse and guidance on breeding/genotyping
492 strategies. We are grateful to Dr. Shonna Johnston and the Flow CoRE facility in the QMRI for their expertise
493 and guidance for FACS experiments. Finally, the authors acknowledge the services of Edinburgh Genomics, as
494 well as Dr. Peter Thorpe at the University of St Andrews for bioinformatics support.

495 **Author Contributions**

496 M.K.M. and M.A.B. conception and design of research; M.K.M., S.R.L., A.R. and H.M.C. performed
497 experiments; M.K.M., S.R.L., H.M.C., A.R. and C.B. analysed the data; M.K.M. prepared figures; M.K.M.
498 drafted the manuscript; M.K.M. and M.A.B. edited and revised manuscript; M.K.M., S.R.L., H.M.C., A.R.,
499 C.B., S.M.W. and M.A.B. approved final version of the manuscript.

500 **Data sharing statement**

501 The raw RNAseq data have been uploaded to the Sequence Read Archive at NCBI, with the project ID:
502 PRJNA820455.

503

504 **Supplemental Material TOC**

505 Supplementary Figure 1. Validation of corticosteroid-induced transcripts in mCCD_{el1} cells.

506 Supplementary Figure 2. Expression of reference genes used for validation of identified corticosteroid-induced
507 transcripts.

508 Supplementary Figure 3. Gating strategy for FACS of primary cells into tdTom and GFP labelled populations.

509 Supplementary Figure 4. Expression of reference genes used for measurement of identified corticosteroid-
510 induced transcripts in primary principal cells.

511 Supplementary Figure 5. Expression of reference genes used for measurement of steroid-induced targets in
512 isolated primary principal cells in mT/mG-Aqp2Cre mice following acute injection of corticosteroids.

513

514

515

516

517

518

519

520

521

522

523

524

525

526

527

528

529

530 **References**

- 531 1. Loffing J, Korbmacher C: Regulated sodium transport in the renal connecting tubule (CNT) via the epithelial
532 sodium channel (ENaC). *Pflugers Archiv European Journal of Physiology*, 458: 111-135, 2009
- 533 2. Hunter RW, Ivy JR, Flatman PW, Kenyon CJ, Craigie E, Mullins LJ, *et al.*: Hypertrophy in the distal
534 convoluted tubule of an 11 β -hydroxysteroid dehydrogenase type 2 knockout model. *Journal of the American*
535 *Society of Nephrology*, 26: 1537-1548, 2015
- 536 3. Maeoka Y, Su XT, Wang WH, Duan XP, Sharma A, Li N, *et al.*: Mineralocorticoid Receptor Antagonists
537 Cause Natriuresis in the Absence of Aldosterone. *Hypertension*, 79: 1423-1434, 2022
- 538 4. Stewart PM, Corrie JET, Shackleton CHL, Edwards CRW: Syndrome of apparent mineralocorticoid excess -
539 a defect in the cortisol cortisone shuttle. *Journal of Clinical Investigation*, 82: 340-349, 1988
- 540 5. Kotelevtsev Y, Brown RW, Fleming S, Kenyon C, Edwards CRW, Seckl JR, *et al.*: Hypertension in mice
541 lacking 11 β -hydroxysteroid dehydrogenase type 2. *Journal of Clinical Investigation*, 103: 683-689, 1999
- 542 6. Hunter R, Ivy JR, Bailey MA: Glucocorticoids and renal Na⁺ transport: implications for hypertension and salt
543 sensitivity. *Journal of Physiology*, 592: 1731-1744, 2014
- 544 7. Verrey F: Transcriptional control of sodium transport in tight epithelia by adrenal steroids. *Journal of*
545 *Membrane Biology*, 144: 93-110, 1995
- 546 8. Shane MA, Nofziger C, Blazer-Yost BL: Hormonal regulation of the epithelial Na⁺ channel: From
547 amphibians to mammals. *General and Comparative Endocrinology*, 147: 85-92, 2006
- 548 9. Muller OG, Parnova RG, Centeno G, Rossier BC, Firsov D, Horisberger JD: Mineralocorticoid effects in the
549 kidney: Correlation between aENaC, GILZ, and Sgk-1 mRNA expression and urinary excretion of Na⁺ and K⁺.
550 *Journal of the American Society of Nephrology*, 14: 1107-1115, 2003
- 551 10. Poulsen SB, Limbutara K, Fenton RA, Pisitkun T, Christensen BM: RNA sequencing of kidney distal tubule
552 cells reveals multiple mediators of chronic aldosterone action. *Physiological Genomics*, 50: 343-354, 2018
- 553 11. Swanson EA, Nelson JW, Jeng S, Erspamer KJ, Yang CL, McWeeney S, *et al.*: Salt-sensitive transcriptome
554 of isolated kidney distal tubule cells. *Physiological Genomics*, 51: 125-135, 2019
- 555 12. Robert-Nicoud M, Flahaut M, Elalouf JM, Nicod M, Salinas M, Bens M, *et al.*: Transcriptome of a mouse
556 kidney cortical collecting duct cell line: Effects of aldosterone and vasopressin. *Proceedings of the National*
557 *Academy of Sciences of the United States of America*, 98: 2712-2716, 2001
- 558 13. Gumz ML, Popp MP, Wingo CS, Cain BD: Early transcriptional effects of aldosterone in a mouse inner
559 medullary collecting duct cell line. *American Journal of Physiology-Renal Physiology*, 285: F664-F673, 2003
- 560 14. Gonzalez-Nunez D, Morales-Ruiz M, Leivas A, Hebert SC, Poch E: In vitro characterization of aldosterone
561 and cAMP effects in mouse distal convoluted tubule cells. *American Journal of Physiology - Renal Physiology*,
562 286: F936-F944, 2004
- 563 15. Alvarez De La Rosa D, Zhang P, N aray-Fejes-T oth A, Fejes-T oth G, Canessa CM: The serum and
564 glucocorticoid kinase sgk increases the abundance of epithelial sodium channels in the plasma membrane of
565 *Xenopus* oocytes. *Journal of Biological Chemistry*, 274: 37834-37839, 1999
- 566 16. Chen SY, Bhargava A, Mastroberardino L, Meijer OC, Wang J, Buse P, *et al.*: Epithelial sodium channel
567 regulated by aldosterone-induced protein sgk. *Proceedings of the National Academy of Sciences of the United*
568 *States of America*, 96: 2514-2519, 1999

- 569 17. Soundararajan R, Zhang TT, Wang J, Vandewalle A, Pearce D: A novel role for glucocorticoid-induced
570 leucine zipper protein in epithelial sodium channel-mediated sodium transport. *Journal of Biological Chemistry*,
571 280: 39970-39981, 2005
- 572 18. Canonica J, Sergi C, Maillard M, Klusonova P, Odermatt A, Koesters R, *et al.*: Adult nephron-specific MR-
573 deficient mice develop a severe renal PHA-1 phenotype. *Pflugers Archiv European Journal of Physiology*, 468:
574 895-908, 2016
- 575 19. Faresse N, Lagnaz D, Debonneville A, Ismailji A, Maillard M, Fejes-Toth G, *et al.*: Inducible kidney-
576 specific Sgk1 knockout mice show a salt-losing phenotype. *American Journal of Physiology - Renal Physiology*,
577 302: F977-F985, 2012
- 578 20. Rashmi P, Colussi G, Ng M, Wu X, Kidwai A, Pearce D: Glucocorticoid-induced leucine zipper protein
579 regulates sodium and potassium balance in the distal nephron. *Kidney International*, 91: 1159-1177, 2017
- 580 21. Fodstad H, Gonzalez-Rodriguez E, Bron S, Gaeggeler H, Guisan B, Rossier BC, *et al.*: Effects of
581 mineralocorticoid and K⁺ concentration on K⁺ secretion and ROMK channel expression in a mouse cortical
582 collecting duct cell line. *American Journal of Physiology - Renal Physiology*, 296: F966-F975, 2009
- 583 22. Gaeggeler HP, Gonzalez-Rodriguez E, Jaeger NF, Loffing-Cueni D, Norregaard R, Loffing J, *et al.*:
584 Mineralocorticoid versus glucocorticoid receptor occupancy mediating aldosterone-stimulated sodium transport
585 in a novel renal cell line. *Journal of the American Society of Nephrology*, 16: 878-891, 2005
- 586 23. Gaeggeler HP, Guillod Y, Loffing-Cueni D, Loffing J, Rossier BC: Vasopressin-dependent coupling
587 between sodium transport and water flow in a mouse cortical collecting duct cell line. *Kidney International*, 79:
588 843-852, 2010
- 589 24. Mansley MK, Neuhuber W, Korbmacher C, Bertog M: Norepinephrine stimulates the epithelial Na⁺ channel
590 in cortical collecting duct cells via α_2 -adrenoceptors. *American Journal of Physiology - Renal Physiology*, 308:
591 F450-F458, 2015
- 592 25. Mansley MK, Wilson SM: Effects of nominally selective inhibitors of the kinases PI3K, SGK1 and PKB on
593 the insulin-dependent control of epithelial Na⁺ absorption. *British Journal of Pharmacology*, 161: 571-588,
594 2010
- 595 26. Martin M: Cutadapt removes adapter sequences from high-throughput sequencing reads. *2011*, 17: 3, 2011
- 596 27. Dobin A, Davis CA, Schlesinger F, Drenkow J, Zaleski C, Jha S, *et al.*: STAR: ultrafast universal RNA-seq
597 aligner. *Bioinformatics*, 29: 15-21, 2013
- 598 28. Robinson MD, McCarthy DJ, Smyth GK: edgeR: a Bioconductor package for differential expression
599 analysis of digital gene expression data. *Bioinformatics*, 26: 139-140, 2010
- 600 29. Nelson RD, Stricklett P, Gustafson C, Stevens A, Ausiello D, Brown D, *et al.*: Expression of an AQP2 Cre
601 recombinase transgene in kidney and male reproductive system of transgenic mice. *American Journal of*
602 *Physiology - Cell Physiology*, 275: C216-C226, 1998
- 603 30. Muzumdar MD, Tasic B, Miyamichi K, Li L, Luo LQ: A global double-fluorescent cre reporter mouse.
604 *Genesis*, 45: 593-605, 2007
- 605 31. O'Sullivan J, Finnie SL, Teenan O, Cairns C, Boyd A, Bailey MA, *et al.*: Refining the mouse subtotal
606 nephrectomy in male 129S2/SV mice for consistent modeling of progressive kidney disease with renal
607 inflammation and cardiac dysfunction. *Frontiers in Physiology*, 10, 2019

- 608 32. Young MJ, Morgan J, Brolin K, Fuller PJ, Funder JW: Activation of mineralocorticoid receptors by
 609 exogenous glucocorticoids and the development of cardiovascular inflammatory responses in adrenalectomized
 610 rats. *Endocrinology*, 151: 2622-2628, 2010
- 611 33. Fakitsas P, Adam G, Daidié D, Van Bemmelen MX, Fouladkou F, Patrignani A, *et al.*: Early aldosterone-
 612 induced gene product regulates the epithelial sodium channel by deubiquitylation. *Journal of the American*
 613 *Society of Nephrology*, 18: 1084-1092, 2007
- 614 34. Schindelin J, Arganda-Carreras I, Frise E, Kaynig V, Longair M, Pietzsch T, *et al.*: Fiji: an open-source
 615 platform for biological-image analysis. *Nat Methods*, 9: 676-682, 2012
- 616 35. Mansley MK, Roe AJ, Francis SL, Gill JH, Bailey MA, Wilson SM: Trichostatin A blocks aldosterone-
 617 induced Na⁺ transport and control of serum- and glucocorticoid-inducible kinase 1 in cortical collecting duct
 618 cells. *British Journal of Pharmacology*, 176: 4708-4719, 2019
- 619 36. Mansley MK, Watt GB, Francis SL, Walker DJ, Land SC, Bailey MA, *et al.*: Dexamethasone and insulin
 620 activate serum and glucocorticoid-inducible kinase 1 (SGK1) via different molecular mechanisms in cortical
 621 collecting duct cells. *Physiological Reports*, 4: e12792, 2016
- 622 37. Mansley MK, Korbmacher C, Bertog M: Inhibitors of the proteasome stimulate the epithelial sodium
 623 channel (ENaC) through SGK1 and mimic the effect of aldosterone. *Pflugers Arch*, 470: 295-304, 2018
- 624 38. Park J, Shrestha R, Qiu CX, Kondo A, Huang SZ, Werth M, *et al.*: Single-cell transcriptomics of the mouse
 625 kidney reveals potential cellular targets of kidney disease. *Science*, 360: 758-763, 2018
- 626 39. Ransick A, Lindstrom NO, Liu J, Zhu Q, Guo JJ, Alvarado GF, *et al.*: Single-cell profiling reveals sex,
 627 lineage, and regional diversity in the mouse kidney. *Developmental Cell*, 51: 399-413, 2019
- 628 40. Bens M, Vallet V, Cluzeaud F, Pascual-Letallec L, Kahn A, Rafestin-Oblin ME, *et al.*: Corticosteroid-
 629 dependent sodium transport in a novel immortalized mouse collecting duct principal cell line. *Journal of the*
 630 *American Society of Nephrology*, 10: 923-934, 1999
- 631 41. Yu MJ, Miller RL, Uawithya P, Rinschen MM, Khositseth S, Braucht DWW, *et al.*: Systems-level analysis
 632 of cell-specific AQP2 gene expression in renal collecting duct. *Proceedings of the National Academy of*
 633 *Sciences of the United States of America*, 106: 2441-2446, 2009
- 634 42. Isobe K, Jung HJ, Yang CR, Claxton J, Sandoval P, Burg MB, *et al.*: Systems-level identification of PKA-
 635 dependent signaling in epithelial cells. *Proceedings of the National Academy of Sciences of the United States of*
 636 *America*, 114: E8875-E8884, 2017
- 637 43. Flores SY, Loffing-Cueni D, Kamynina E, Daidié D, Gerbex C, Chabanel S, *et al.*: Aldosterone-induced
 638 serum and glucocorticoid-induced kinase 1 expression is accompanied by Nedd4-2 phosphorylation and
 639 increased Na⁺ transport in cortical collecting duct cells. *Journal of the American Society of Nephrology*, 16:
 640 2279-2287, 2005
- 641 44. Auberson M, Hoffman-Pochon N, Vandewalle A, Kellenberger S, Schild L: Epithelial Na⁺ channel mutants
 642 causing Liddle's syndrome retain ability to respond to aldosterone and vasopressin. *American Journal of*
 643 *Physiology - Renal Physiology*, 285: F459-F471, 2003
- 644 45. Náray-Fejes-Tóth A, Canessa C, Cleaveland ES, Aldrich G, Fejes-Tóth G: *sgk* is an aldosterone-induced
 645 kinase in the renal collecting duct. Effects on epithelial Na⁺ channels. *Journal of Biological Chemistry*, 274:
 646 16973-16978, 1999

- 647 46. Naray-Fejes-Toth A, Boyd C, Fejes-Toth G: Regulation of epithelial sodium transport by promyelocytic
648 leukemia zinc finger protein. *American Journal of Physiology - Renal Physiology*, 295: F18-F26, 2008
- 649 47. Kamynina E, Dedonneville C, Dens M, Vandewalle A, Staub O: A novel mouse Nedd4 protein suppresses
650 the activity of the epithelial Na⁺ channel. *FASEB Journal*, 15: 204-214, 2001
- 651 48. Cheval L, Van Huyen JPD, Bruneval P, Verbavatz JM, Elalouf JM, Doucet A: Plasticity of mouse renal
652 collecting duct in response to potassium depletion. *Physiological Genomics*, 19: 61-73, 2004
- 653 49. Saxena V, Fitch J, Ketz J, White P, Wetzel A, Chanley MA, *et al.*: Whole Transcriptome Analysis of Renal
654 Intercalated Cells Predicts Lipopolysaccharide Mediated Inhibition of Retinoid X Receptor alpha Function.
655 *Scientific Reports*, 9, 2019
- 656 50. Spindler B, Mastroberardino L, Custer M, Verrey F: Characterization of early aldosterone-induced RNAs
657 identified in A6 kidney epithelia. *Pflugers Arch*, 434: 323-331, 1997
- 658 51. Mastroberardino L, Spindler B, Forster I, Loffing J, Assandri R, May A, *et al.*: Ras pathway activates
659 epithelial Na⁺ channel and decreases its surface expression in *Xenopus* oocytes. *Molecular Biology of the Cell*,
660 9: 3417-3427, 1998
- 661 52. Mueller JW, Gilligan LC, Idkowiak J, Arlt W, Foster PA: The Regulation of Steroid Action by Sulfation and
662 Desulfation. *Endocrine Reviews*, 36: 526-563, 2015
- 663 53. Cole GB, Keum G, Liu J, Small GW, Satyamurthy N, Kepe V, *et al.*: Specific estrogen sulfotransferase
664 (SULT1E1) substrates and molecular imaging probe candidates. *Proceedings of the National Academy of
665 Sciences of the United States of America*, 107: 6222-6227, 2010
- 666 54. Shimada M, Terazawa R, Kamiyama Y, Honma W, Nagata K, Yamazoe Y: Unique properties of a renal
667 sulfotransferase, st1d1, in dopamine metabolism. *Journal of Pharmacology and Experimental Therapeutics*,
668 310: 808-814, 2004
- 669 55. Staub O, Loffing J: Mineralocorticoid action in the aldosterone sensitive distal nephron. In: *Seldin and
670 Giebisch's The Kidney - Physiology and Pathophysiology*. 5th Ed. edited by Alpern M, Caplan, M. and Moe, O.,
671 London, Academic Press, 2013, pp 1181-1211
- 672 56. Funder JW, Pearce PT, Smith R, Smith AI: Mineralocorticoid action: Target tissue specificity is enzyme, not
673 receptor, mediated. *Science*, 242: 583-585, 1988
- 674 57. Bailey MA, Unwin RJ, Shirley DG: In vivo inhibition of renal 11b-hydroxysteroid dehydrogenase in the rat
675 stimulates collecting duct sodium reabsorption. *Clinical Science*, 101: 195-198, 2001
- 676 58. Nesterov V, Dahlmann A, Krueger B, Bertog M, Loffing J, Korbmacher C: Aldosterone-dependent and -
677 independent regulation of the epithelial sodium channel (ENaC) in mouse distal nephron. *American Journal of
678 Physiology - Renal Physiology*, 303: F1289-F1299, 2012
- 679 59. Wu P, Gao Z-X, Zhang D-D, Duan X-P, Terker AS, Lin D-H, *et al.*: Effect of angiotensin II on ENaC in the
680 distal convoluted tubule and in the cortical collecting duct of mineralocorticoid receptor deficient mice. *Journal
681 of the American Heart Association*, 9, 2020
- 682 60. Bertog M, Cuffe JE, Pradervand S, Hummler E, Hartner A, Porst M, *et al.*: Aldosterone responsiveness of
683 the epithelial sodium channel (ENaC) in colon is increased in a mouse model for Liddle's syndrome. *Journal of
684 Physiology*, 586: 459-475, 2008

- 685 61. Nesterov V, Bertog M, Canonica J, Hummler E, Coleman R, Welling PA, *et al.*: Critical role of the
686 mineralocorticoid receptor in aldosterone-dependent and aldosterone-independent regulation of ENaC in the
687 distal nephron. *American Journal of Physiology - Renal Physiology*, 321: F257-F268, 2021
- 688 62. Bostonjoglo M, Reeves WB, Reilly RF, Velazquez H, Robertson N, Litwack G, *et al.*: 11 beta-
689 hydroxysteroid dehydrogenase, mineralocorticoid receptor, and thiazide-sensitive Na-Cl cotransporter
690 expression by distal tubules. *Journal of the American Society of Nephrology*, 9: 1347-1358, 1998
- 691 63. Chen LH, Chou CL, Knepper MA: Targeted Single-Cell RNA-seq Identifies Minority Cell Types of Kidney
692 Distal Nephron. *Journal of the American Society of Nephrology*, 32: 886-896, 2021
- 693 64. Labarca M, Nizar JM, Walczak EM, Dong WX, Pao AC, Bhalla V: Harvest and primary culture of the
694 murine aldosterone-sensitive distal nephron. *American Journal of Physiology - Renal Physiology*, 308: F1306-
695 F1315, 2015
- 696 65. Assmus AM, Mansley MK, Mullins LJ, Peter A, Mullins JJ: mCCD(c11) cells show plasticity consistent
697 with the ability to transition between principal and intercalated cells. *American Journal of Physiology - Renal
698 Physiology*, 314: F820-F831, 2018
- 699 66. Guo QS, Wang YQ, Tripathi P, Manda KR, Mukherjee M, Chaklader M, *et al.*: Adam10 mediates the choice
700 between principal cells and intercalated cells in the kidney. *Journal of the American Society of Nephrology*, 26:
701 149-159, 2015
- 702 67. Rupprecht R, Reul J, Vansteensel B, Spengler D, Soder M, Berning B, *et al.*: Pharmacological and
703 functional characterization of human mineralocorticoid and glucocorticoid receptor ligands. *Eur J Pharmacol-
704 Molec Pharmacol Sect*, 247: 145-154, 1993
- 705 68. Young MJ, Moussa L, Dille R, Funder JW: Early inflammatory responses in experimental cardiac
706 hypertrophy and fibrosis: Effects of 11 beta-hydroxysteroid dehydrogenase inactivation. *Endocrinology*, 144:
707 1121-1125, 2003

708 **Tables**709 **Table 1. Differential analysis of gene expression following acute corticosteroid treatment of mCCD_{cl1} cells.**

Experimental conditions compared	Upregulated genes	Downregulated genes
Vehicle <i>vs.</i> Aldosterone	8	1
Vehicle <i>vs.</i> Corticosterone	0	0
Vehicle <i>vs.</i> CBX + Corticosterone	123	78
Aldosterone <i>vs.</i> CBX + Corticosterone	64	7
Corticosterone <i>vs.</i> CBX + Corticosterone	82	22

710 Number of genes up or downregulated in each contrast made of experimental condition according to the
 711 thresholds on minimum log₂ fold change (1) and maximum false discovery rate (0.05).

712

713

714

715

716

717

718

719

720

721

722

723

724

725

726

727

728

729

730

731 **Table 2. Differentially expressed genes in mCCD_{cl1} cells following aldosterone treatment.**

Upregulated genes (Veh vs. Aldo)			
Gene Symbol	Gene Name	Log₂FC	FDR
<i>Zbtb16</i>	Zinc finger and BTB domain-containing 16	3.2	6.0 x 10 ⁻¹²
<i>Sgk1</i>	Serum and glucocorticoid-regulated kinase 1	2.9	0.0001
<i>Tslp</i>	Thymic stromal lymphopoietin	2.1	0.0477
<i>Rasd1</i>	Ras related dexamethasone-induced 1	2.1	9.4 x 10 ⁻¹⁰
<i>Gm16178</i>	N/A	1.6	0.0007
<i>Sult1d1</i>	Sulfotransferase family 1D, member 1	1.1	3.2 x 10 ⁻¹⁴
<i>Gm43305</i>	N/A	1.1	0.0002
<i>Defbl</i>	Defensin beta 1	1.0	0.0005
Downregulated transcripts (Veh vs. Aldo)			
Gene Symbol	Gene Name	Log₂FC	FDR
<i>Gm9694</i>	N/A	-3.0	0.0444

732 The threshold for False Discovery Rate (FDR) was 0.05 and the Log₂ fold change (Log₂FC) threshold was 1.

733

734

735

736

737

738

739

740

741

742

743

744

745

746

747

748

749 **Table 3. Differentially expressed genes in mCCD_{cl1} cells following corticosterone treatment, in the absence**
 750 **of 11 β HSD2 activity.**

Top 15 upregulated annotated genes (Veh vs. CBX+cort)			
Gene Symbol	Gene Name	Log₂FC	FDR
<i>Zbtb16</i>	Zinc finger and BTB domain-containing 16	5.7	7.4 x 10 ⁻¹⁸
<i>Sgk1</i>	Serum and glucocorticoid-regulated kinase 1	5.6	3.1 x 10 ⁻⁸
<i>Rasd1</i>	Ras related dexamethasone-induced 1	4.2	7.0 x 10 ⁻¹⁹
<i>Hif3a</i>	Hypoxia inducible factor 3, alpha subunit	2.7	1.1 x 10 ⁻¹⁴
<i>Sult1a1</i>	Sulfotransferase family 1A, phenol-preferring, member 1	2.7	0.0005
<i>Sult1d1</i>	Sulfotransferase family 1D, member 1	2.6	3.0 x 10 ⁻¹⁰
<i>Tsc22d3</i>	TSC22 domain family, member 3	2.5	1.2 x 10 ⁻⁸
<i>Myom2</i>	Myomesin 2	2.5	0.0031
<i>Htr6</i>	5-Hydroxytryptamine receptor 6	2.4	0.0198
<i>Slco4c1</i>	Solute carrier organic anion transporter family, member 4C1	2.3	0.0012
<i>Tekt4</i>	Tektin 4	2.2	4.1 x 10 ⁻⁵
<i>Per1</i>	Period circadian clock 1	2.1	5.3 x 10 ⁻⁶
<i>Abcb5</i>	ATP-binding cassette, sub-family B (MDR/TAP), member 5	2.1	2.4 x 10 ⁻¹¹
<i>Adora2b</i>	Adenosine A2b receptor	2.1	6.4 x 10 ⁻⁹
<i>Arg2</i>	Arginase type II	2.1	1.3 x 10 ⁻¹²
All downregulated annotated genes (Veh vs. CBX+cort)			
Gene Symbol	Gene Name	Log₂FC	FDR
<i>Hao2</i>	Hydroxyacid oxidase 2	-2.2	6.8 x 10 ⁻⁶
<i>Lipc</i>	Lipase, hepatic	-1.8	0.0210
<i>Il1f6</i>	Interleukin 1 family, member 6	-1.7	0.0012
<i>Mboat4</i>	Membrane bound O-acyltransferase domain containing 4	-1.5	0.0026
<i>Pabpn1l</i>	Poly(A) binding protein nuclear 1-like	-1.4	8.5 x 10 ⁻⁶
<i>Sprr2g</i>	Small proline-rich protein 2G	-1.3	0.0348
<i>Prl2c5</i>	Prolactin family 2, subfamily c, member 5	-1.3	0.0305
<i>Gimap1</i>	GTPase, IMAP family member 1	-1.2	0.0364
<i>Id4</i>	Inhibitor of DNA binding 4	-1.2	0.0276

751 The threshold for false discovery rate (FDR) was 0.05 and the log₂ fold change (Log₂FC) threshold was 1. For
 752 clarity only annotated genes are shown, a full list can be found in the supplemental excel file.

753

754

755

756

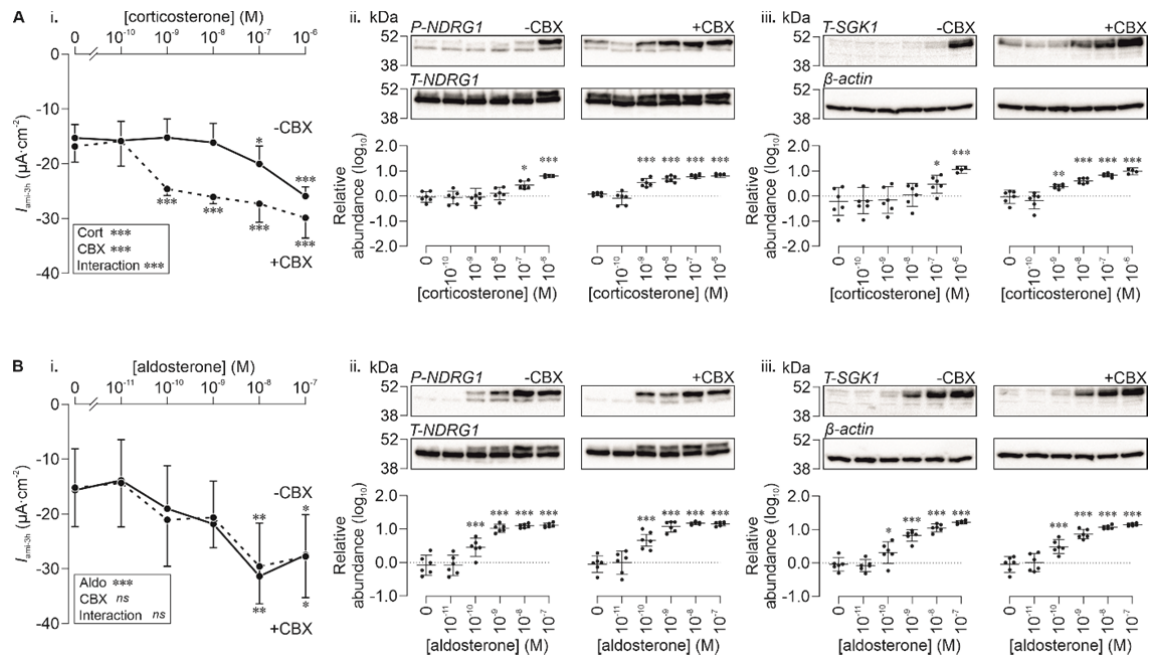
757

758

759 Table 4. Validation of isolated primary CD cells by qRT-PCR.

Tubule-specific target	Symbol	Nephron segment	tdTom population		GFP population		Cq range of standards	Population enriched?
			Cq	Expression of GOI relative to reference genes (log ₁₀)	Cq	Expression of GOI relative to reference genes (log ₁₀)		
NHE3	<i>Slc9a3</i>	Proximal tubule	30.6 ± 1.2	0.56 ± 0.47	34.4 ± 0.5	-0.91 ± 0.34***	29.3-34.7	tdTom
NKCC2	<i>Slc12a1</i>	Loop of Henle	30.3 ± 1.0	-0.03 ± 0.18	32.3 ± 0.8	-3.00 ± 3.81**	26.9-32.4	tdTom
NCC	<i>Slc12a3</i>	Distal Convoluted Tubule	30.4 ± 1.3	-0.47 ± 0.10	29.0 ± 0.6	-0.33 ± 0.13	25.1-30.7	-
11βHSD2	<i>Hsd11b2</i>	Collecting duct – principal cell	BLD	BLD	25.8 ± 0.7	0.09 ± 0.11	23.6-29.1	GFP
α-ENaC	<i>Scnn1a</i>	Collecting duct – principal cell	BLD	BLD	31.2 ± 0.8	-0.10 ± 0.18	29.1-32.8	GFP
ROMK	<i>Kcnj1</i>	Collecting duct – principal cell	BLD	BLD	33.7 ± 0.6	-0.02 ± 0.16	32.4-35.1	GFP
Pendrin	<i>Slc26a4</i>	Collecting duct – β-intercalated cell	BLD	BLD	30.5 ± 0.8	-0.02 ± 0.14	27.4-33.1	GFP
AE1	<i>Slc4a1</i>	Collecting duct – α-intercalated cell	35.4 ± 0.9	-0.48 ± 0.38	34.8 ± 0.7	-0.33 ± 0.29	29.7-35.7	-
V-ATPase β1	<i>Atp6v1b1</i>	Collecting duct – α - and β-intercalated cell	BLD	BLD	32.2 ± 0.6	-0.06 ± 0.14	28.4-34.2	GFP
UT-A1	<i>Slc14a2</i>	Medullary collecting duct	BLD	BLD	31.9 ± 0.8	0.20 ± 0.22	29.1-35.2	GFP
			tdTom population		GFP population			
Reference gene	Symbol		Cq	Expression (log ₁₀)	Cq	Expression (log ₁₀)	Cq range of standards	Population enriched?
β-actin	<i>Actb1</i>	Reference gene	28.7 ± 1.1	-1.13 ± 0.43	27.6 ± 0.7	-0.68 ± 0.27	26.1-30.9	-
18S	<i>Rn18s</i>	Reference gene	15.7 ± 1.4	-1.12 ± 0.46	15.6 ± 0.7	-1.13 ± 0.36	13.1-18.2	-

760 Expression of nephron segment-specific genes in either tdTom-labelled (n = 5) or GFP-labelled (n = 5) populations of cells isolated by FACS. For each gene of interest
761 (GOI), both the Cq (cycle quantification value) and transcript expression relative to the average expression of reference genes (log₁₀) is shown. The range of Cq values
762 detected across the 7-point standards is also shown. The population where the GOI was found to be enriched, determined either by statistical significance of the relative
763 expression (log₁₀) or where one population showed expression within the 7 point standard and the other was below the limit of detection (BLD), is highlighted in the final
764 column. A hyphen denotes no difference in gene expression between tdTom and GFP populations. Statistical significance was determined by unpaired t-test, ** p < 0.01,
765 *** p < 0.001.

766 **Figures and figure legends**

767

768 **Figure 1. Effects of acute corticosteroids on ENaC-mediated transport and SGK1 activity and expression**
 769 **in mCCD_{cl1} cells.** Amiloride-sensitive currents measured from polarised mCCD_{cl1} cells after 3h (I_{ami-3h})
 770 exposure to increasing concentrations of corticosterone (Ai) or aldosterone (Bi) in the absence (-CBX, solid
 771 line) or presence (+CBX, dashed line) of carbenoxolone (10 μ M, 30 min preincubation), to inhibit 11 β HSD2
 772 activity. H₂O was used as vehicle control for CBX, amiloride (10 μ M, 10 min) was added following
 773 corticosteroid treatment. The activity (ii) and expression (iii) of SGK1 was determined by measuring the
 774 abundance of P-NDRG1 or T-SGK1, respectively, in cell lysates following corticosteroid treatment and
 775 electrophysiological measurements. These are expressed relative to T-NDRG1 and β -actin, respectively. Upper
 776 panels show representative blots and lower panels show densitometric data expressed as a fold change from the
 777 control (0) lane (\log_{10}). Data are shown as mean \pm 95% CI ($n = 7$). Statistical significance was determined by a
 778 two-way ANOVA for the electrophysiological data, with a Dunnett's post-hoc test, and a one-way ANOVA for
 779 Western blot data, due to separate blots for - and + CBX, with a Dunnett's post-hoc test.

780

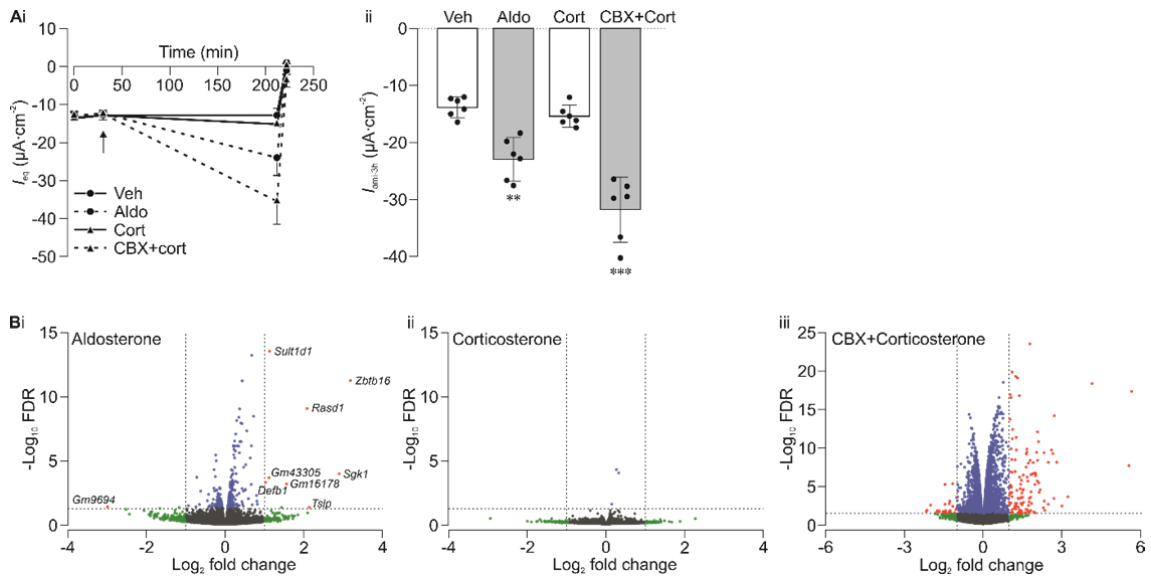
781

782

783

784

785



786

787 **Figure 2. Differentially expressed transcripts in corticosteroid-treated mCCD_{cl1} cells.** (Ai) I_{eq} measured
 788 from cells treated with either solvent vehicle (Veh), 3 nM aldosterone (Aldo), or 100 nM corticosterone (Cort)
 789 for 3 h, arrow indicates addition of corticosteroid. An additional corticosterone group was pre-treated
 790 carbenoxolone (CBX) (10 μM , 30 min), all other groups received vehicle control for this period. Amiloride
 791 (10 μM) was added to the apical bath for a final 10 min, (ii) shows the amiloride-sensitive current (I_{ami-3h}). Data
 792 are shown as mean \pm 95% CI (left panel) and as individual points and mean \pm 95% CI (right panel). Statistical
 793 significance was determined by one-way ANOVA with a Tukey's post-hoc test used to compare groups to
 794 vehicle control, ** $p < 0.01$, *** $p < 0.001$. (B) Differentially expressed transcripts are plotted as \log_2 fold change
 795 versus $-\log_{10}$ false discovery rate (FDR). The horizontal dashed line represents the specified FDR threshold
 796 (0.05) and the vertical dashed lines indicate the specified fold change threshold (2) in both positive and negative
 797 directions. Each treatment: (Bi) aldosterone, (ii) corticosterone or (iii) CBX+corticosterone, is compared to
 798 vehicle-treated control. Points passing only the FDR threshold are shown in green, passing only the fold change
 799 threshold are shown in blue and those passing both thresholds are shown in red. Individual transcripts passing
 800 both thresholds in aldosterone-treated cells are labelled.

801

802

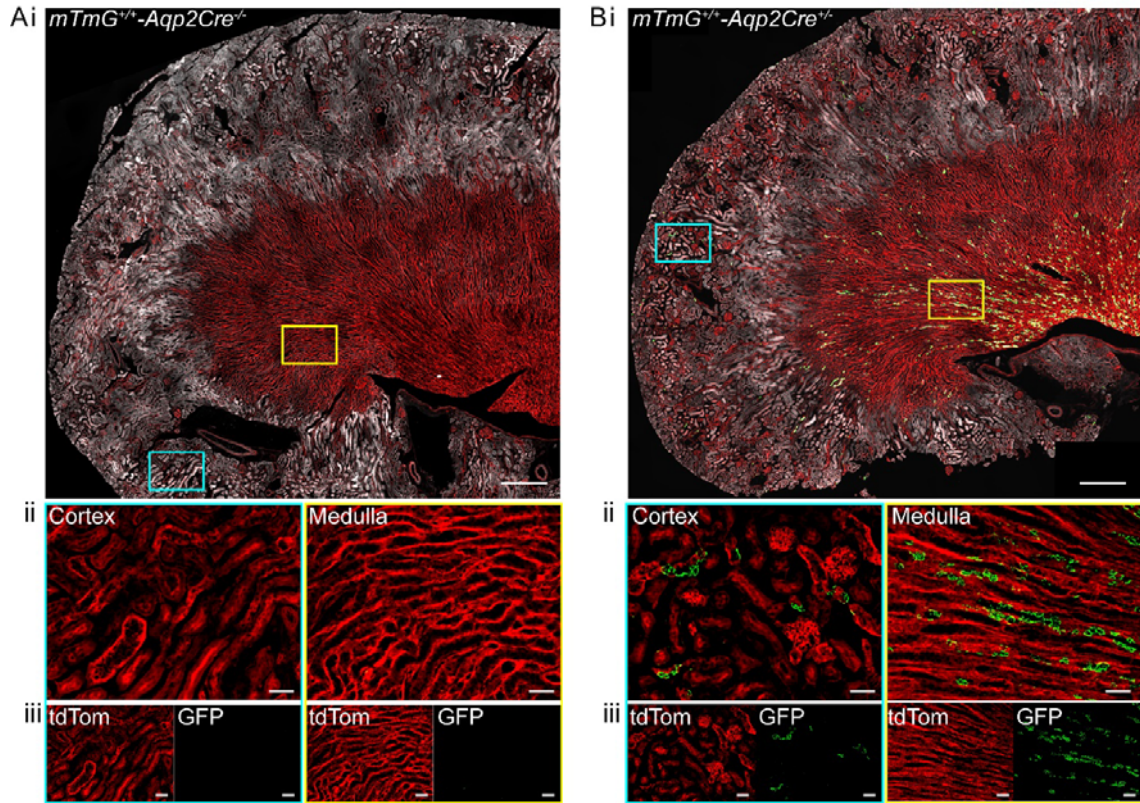
803

804

805

806

807



808

809 **Figure 3. tdTom and GFP expression in kidney sections from mTmG-Aqp2Cre mice.** Longitudinal sections
 810 of fixed kidneys from adult mTmG^{+/+}-Aqp2Cre^{-/-} mice (A) and mTmG^{+/+}-Aqp2Cre^{+/-} mice (B) showing tdTom
 811 and GFP labelling. (i) Tiled images taken with 40X objective across the section with 488 nm (grey:
 812 autofluorescence to show tissue morphology, green: GFP signal) and 555 nm (red: tdTomato signal) excitation
 813 light. (ii) Cortex and medullary regions are shown at higher magnification, regions of interest denoted in (i) by
 814 cyan and yellow boxes, respectively. (iii) Individual 555 nm and 488 nm channels for (ii) are shown. Scale bars:
 815 (i) 500 μ m, (ii-iii) 50 μ m.

816

817

818

819

820

821

822

823

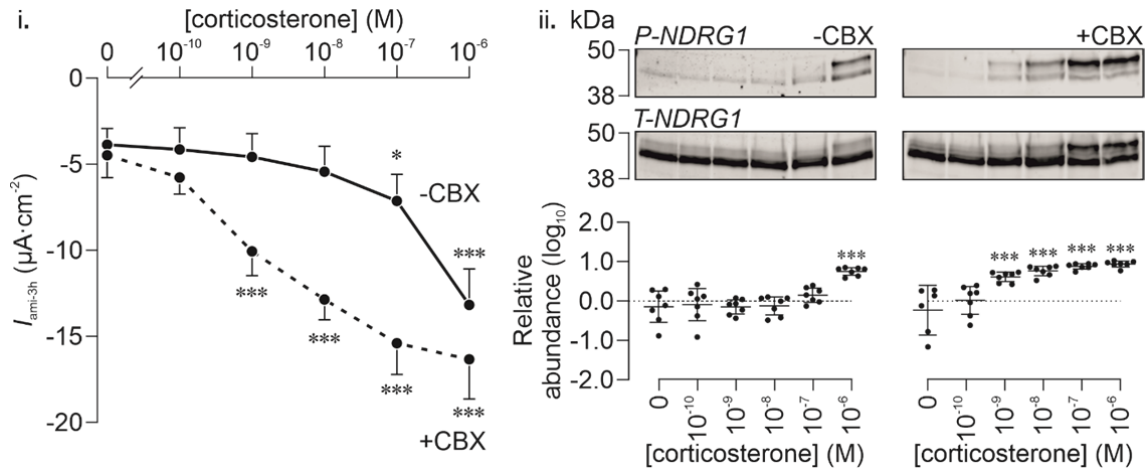


Figure 4. Effects of acute addition of corticosterone on ENaC-mediated transport and SGK1 activity and expression in cultured primary principal cells. (i) Amiloride-sensitive currents were determined in primary principal cells after 3h (I_{ami-3h}) exposure to increasing concentrations of corticosterone in the absence (-CBX) or presence (+CBX) of carbenoxolone (10 μ M, 30 min preincubation), to inhibit 11 β HSD2 activity. H₂O was used as vehicle control for CBX, amiloride (10 μ M, 10 min) was added following corticosteroid treatment. (ii) The activity of SGK1 was determined by measuring the abundance of P-NDRG1 in cell lysates following corticosteroid treatment and electrophysiological measurements, expressed relative to T-NDRG1. Upper panels show representative blots and lower panels show densitometric data expressed as a fold change from the control (0) lane (\log_{10}). Data are shown as mean \pm 95% CI ($n = 7$). Statistical significance was determined by a two-way ANOVA for the electrophysiological data and a one-way ANOVA for Western blot data, due to separate blots for - and + CBX, with a Dunnet's post-hoc test, *** $p < 0.001$.

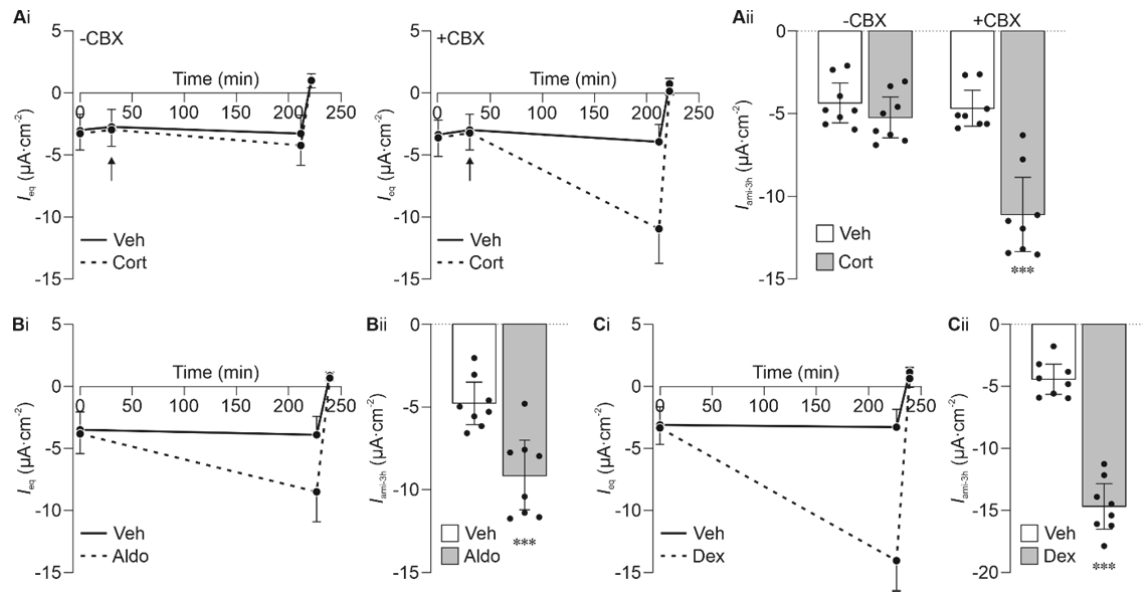


Figure 5. Corticosteroids stimulate ENaC-mediated Na^+ transport in cultured primary principal cells. I_{eq} was measured across polarised monolayers of primary principal cells following treatment with corticosteroids. (A) Cells were pre-incubated with H_2O (-CBX, left) or $10\ \mu\text{M}$ carbenoxolone (+CBX, right) for 30 min. Corticosterone (Cort, $10\ \text{nM}$, dashed line) or solvent vehicle (solid line) was subsequently added for 3 h, arrow denotes addition. (B) Aldosterone (Aldo, $3\ \text{nM}$, dashed line) and (C) dexamethasone (Dex, $100\ \text{nM}$, dashed line), or respective solvent vehicle (solid line), were added to cells for 3 h. In all experiments, amiloride ($10\ \mu\text{M}$) was subsequently applied for 10 min. Data shown in traces (Ai, Bi, Ci) are mean $I_{eq} \pm 95\%$ CI and in bar graphs (Aii, Bii, Cii) as individual points and mean $I_{ami-3h} \pm 95\%$ CI ($n = 8$). Statistical significance in (A) was determined by two-way ANOVA and Tukey's post hoc test and in (B) and (C) by unpaired t-test, *** $p < 0.001$.

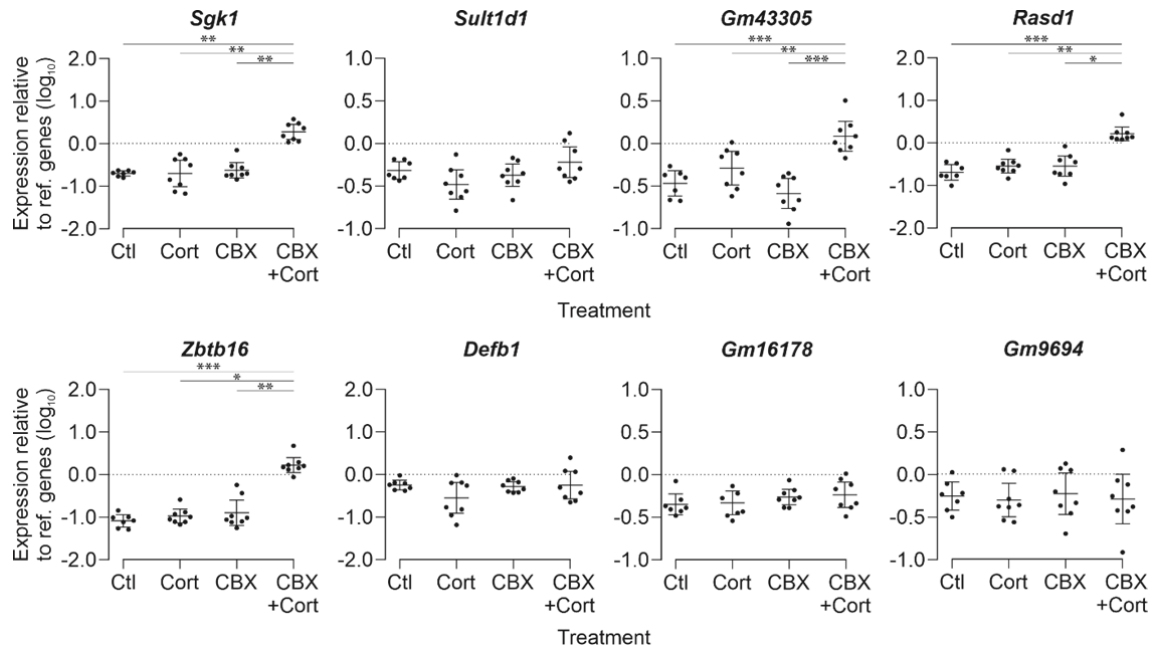


Figure 6. Expression of identified corticosteroid-induced transcripts in primary principal cells treated with corticosterone. Cells were treated with carbenoxolone (CBX) or solvent vehicle for 30 min before addition of corticosterone (Cort, 10 nM) or solvent vehicle for a further 3 h. Amiloride (10 μ M) was added for a final 10 min. Transcript expression of GOI is relative to the average expression of reference genes (\log_{10}): *Actb1* and *Hprt*. Data are shown as individual points and mean \pm 95% CI and GOI is indicated in bold italics above each graph. Statistical significance was determined by one-way ANOVA with Tukey's post-hoc test or Kruskal-Wallis test with Dunn's post-hoc test, where appropriate, * p <0.05, ** p <0.01, *** p <0.001.

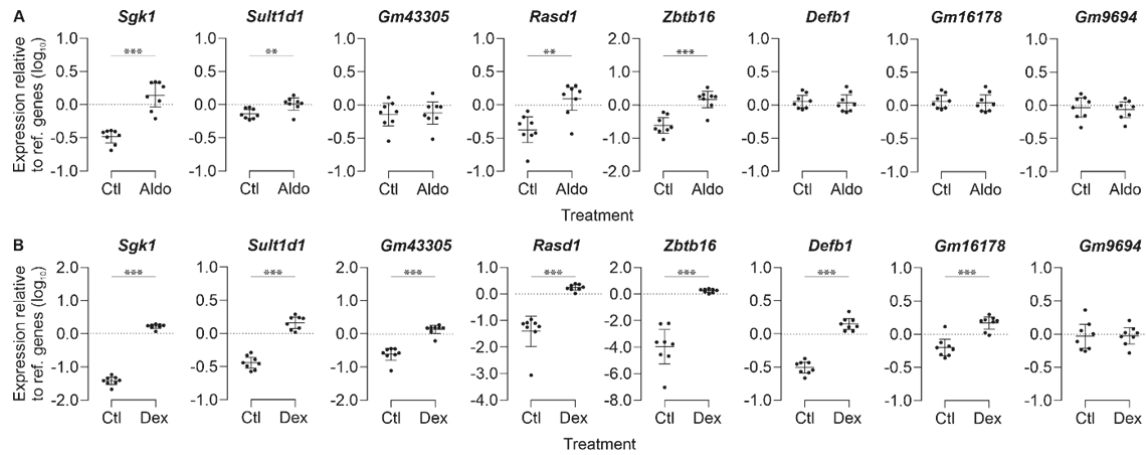


Figure 7. Expression of identified corticosteroid-induced transcripts in primary principal cells treated with aldosterone or dexamethasone. Polarised primary principal cells were treated with either (A) aldosterone (Aldo, 3 nM) or (B) dexamethasone (Dex, 100 nM) for 3 h. Amiloride (10 μ M) was added for a final 10 min. Transcript expression of GOI is relative to the average expression of reference genes (\log_{10}): *Rn18s* and *Tbp* (Aldo) or *Rn18s*, *Tbp* and *Hprt* (Dex). Data are shown as individual points and mean \pm 95% CI and GOI is indicated in bold italics above each graph. Statistical significance was determined by unpaired t-test or Mann-Whitney test, where appropriate, ** p <0.01, *** p <0.001.

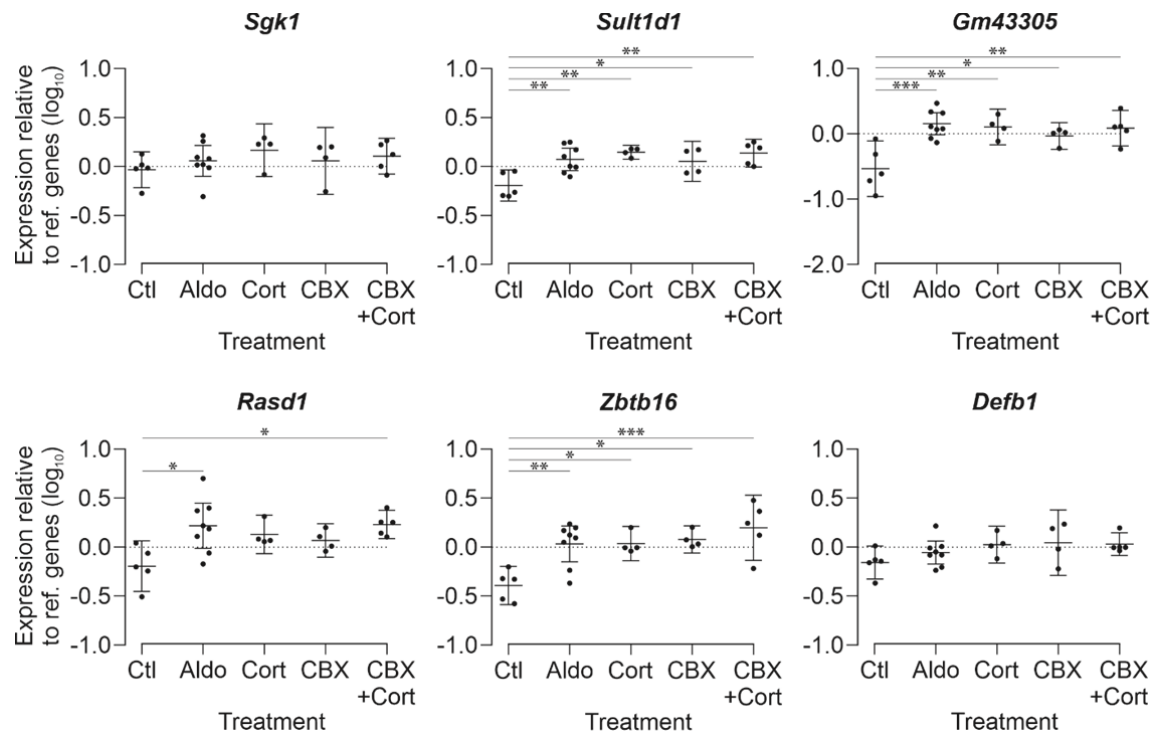


Figure 8. Steroid-induced transcript expression in isolated primary principal cells following acute injection of corticosteroids. Expression of selected target genes were quantified in cells isolated from mT/mG-Aqp2Cre mice 3 h after *ip* injection of solvent vehicle (Ctl), aldosterone (Aldo), corticosterone (Cort), following 8 days *ad lib* access to H₂O. Two further groups were concomitantly treated with carbenoxolone (2.5mg/kg BW/day *po*) for 8 days with subsequent *ip* injection of solvent vehicle (CBX) or corticosterone (CBX+Cort) for 3 h. Target genes were selected from both aldosterone-induced genes identified in the RNA sequencing dataset. Transcript expression of GOI is relative to the average expression of reference genes (log₁₀): *Rn18S* and *Tbp*. Data are shown as individual points and mean ± 95% CI and GOI is indicated in bold italics above each graph. Statistical significance was determined by one-way ANOVA with Tukey's post-hoc test or Kruskal-Wallis test with Dunn's post-hoc test, where appropriate, **p*<0.05, ***p*<0.01, ****p*<0.001.

Figure 1

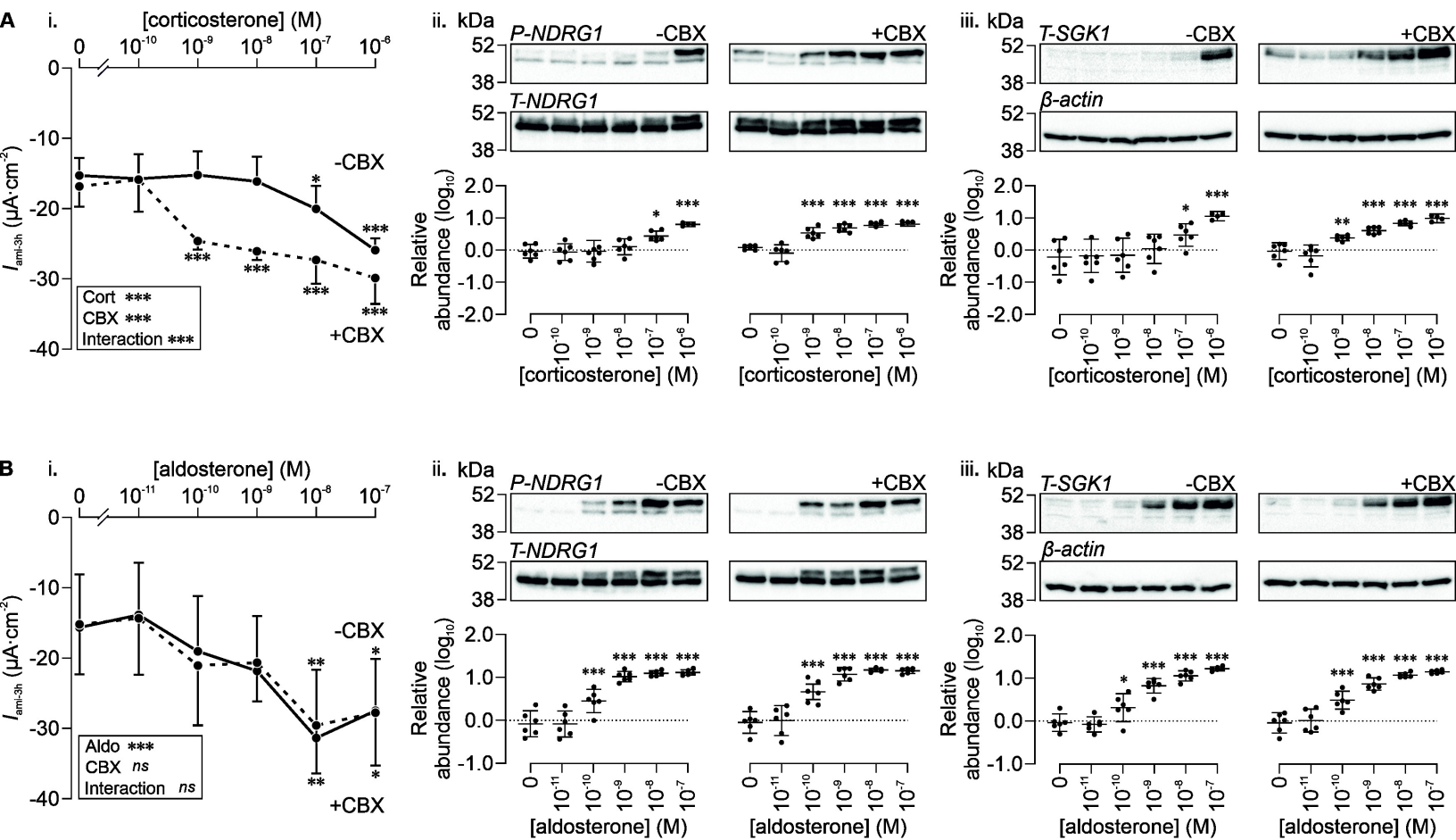


Figure 2

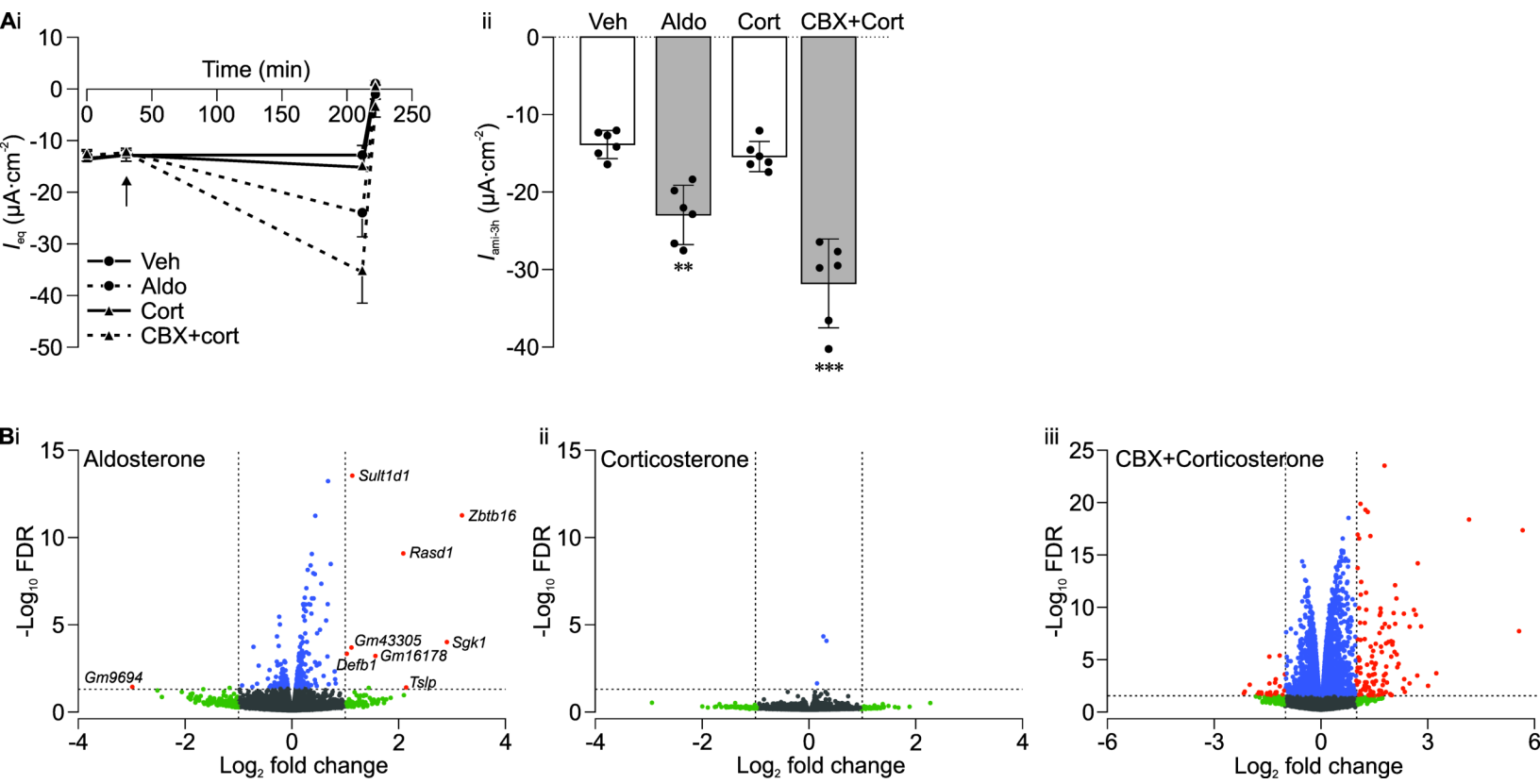


Figure 3

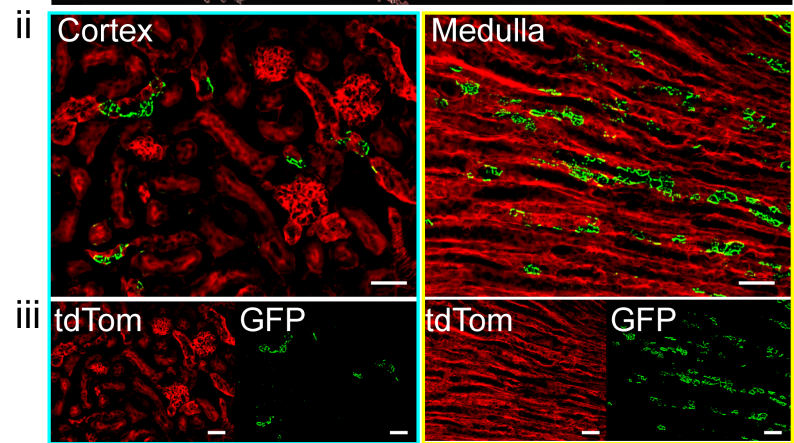
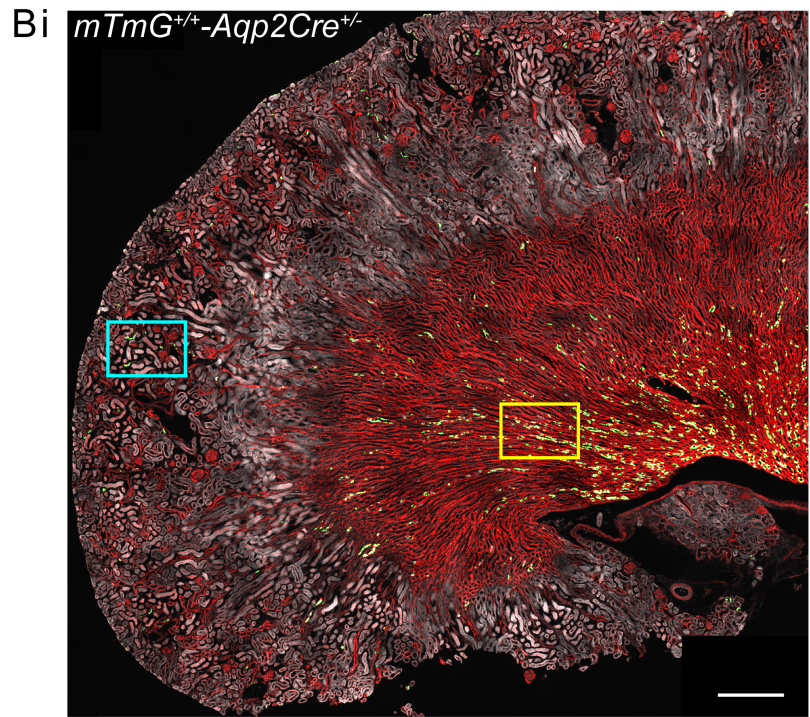
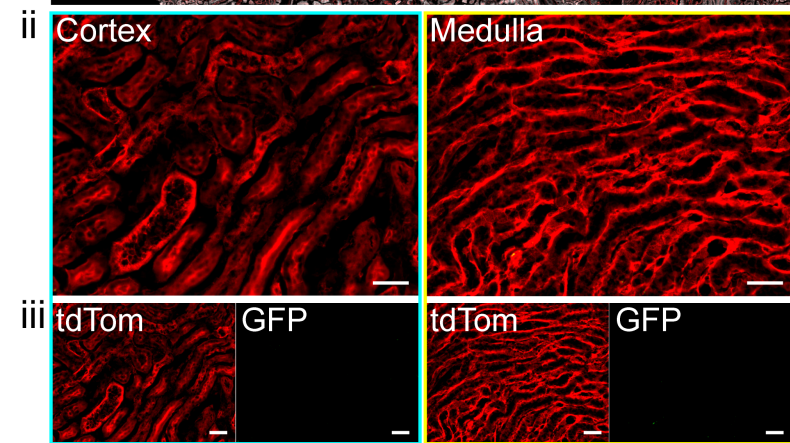
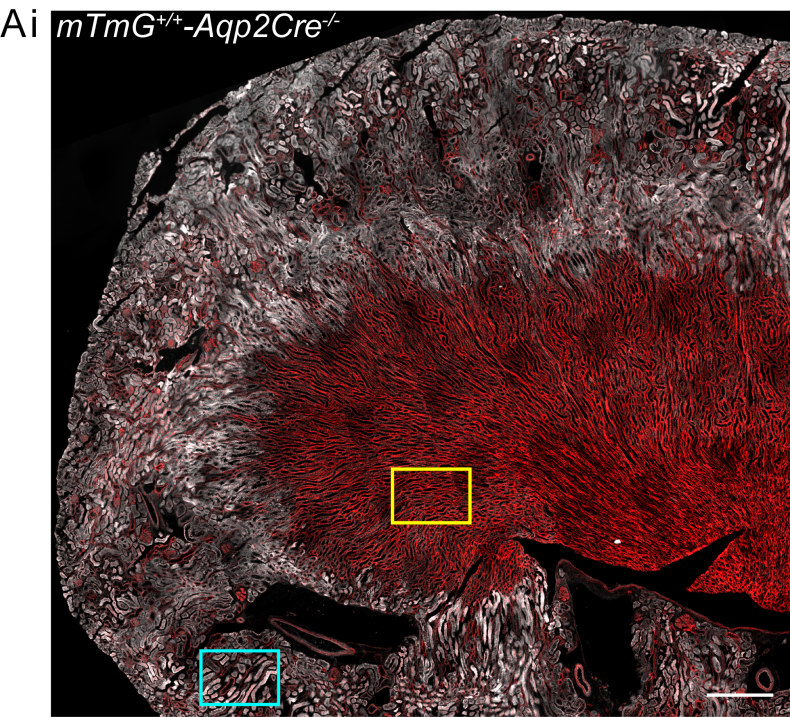


Figure 4

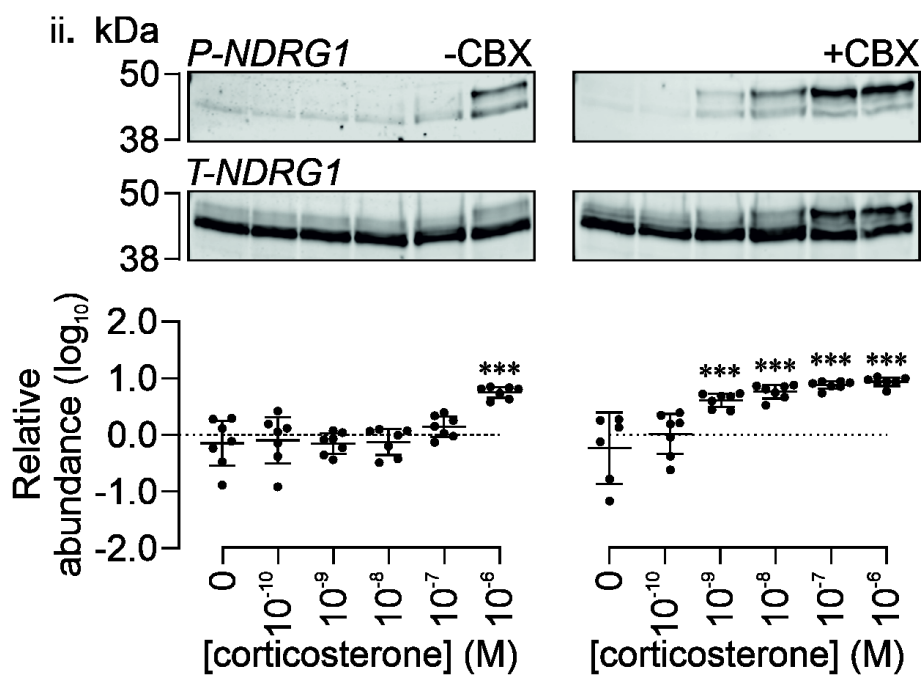
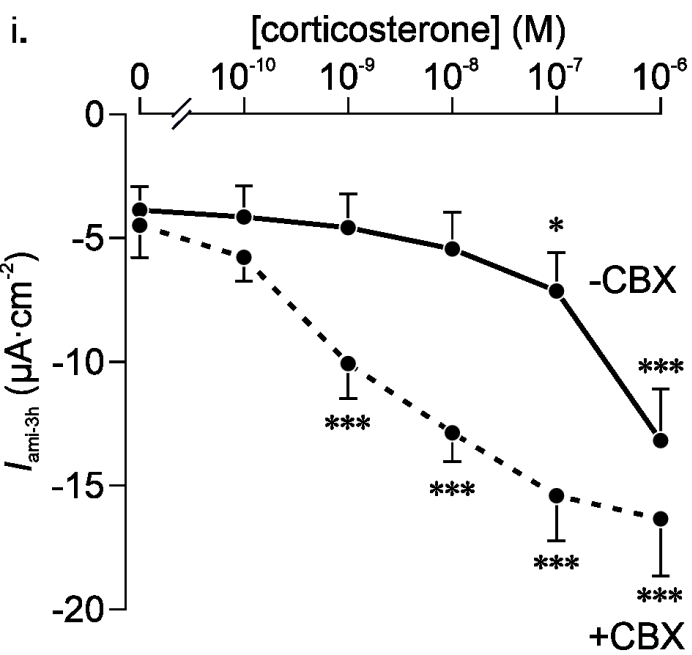


Figure 5

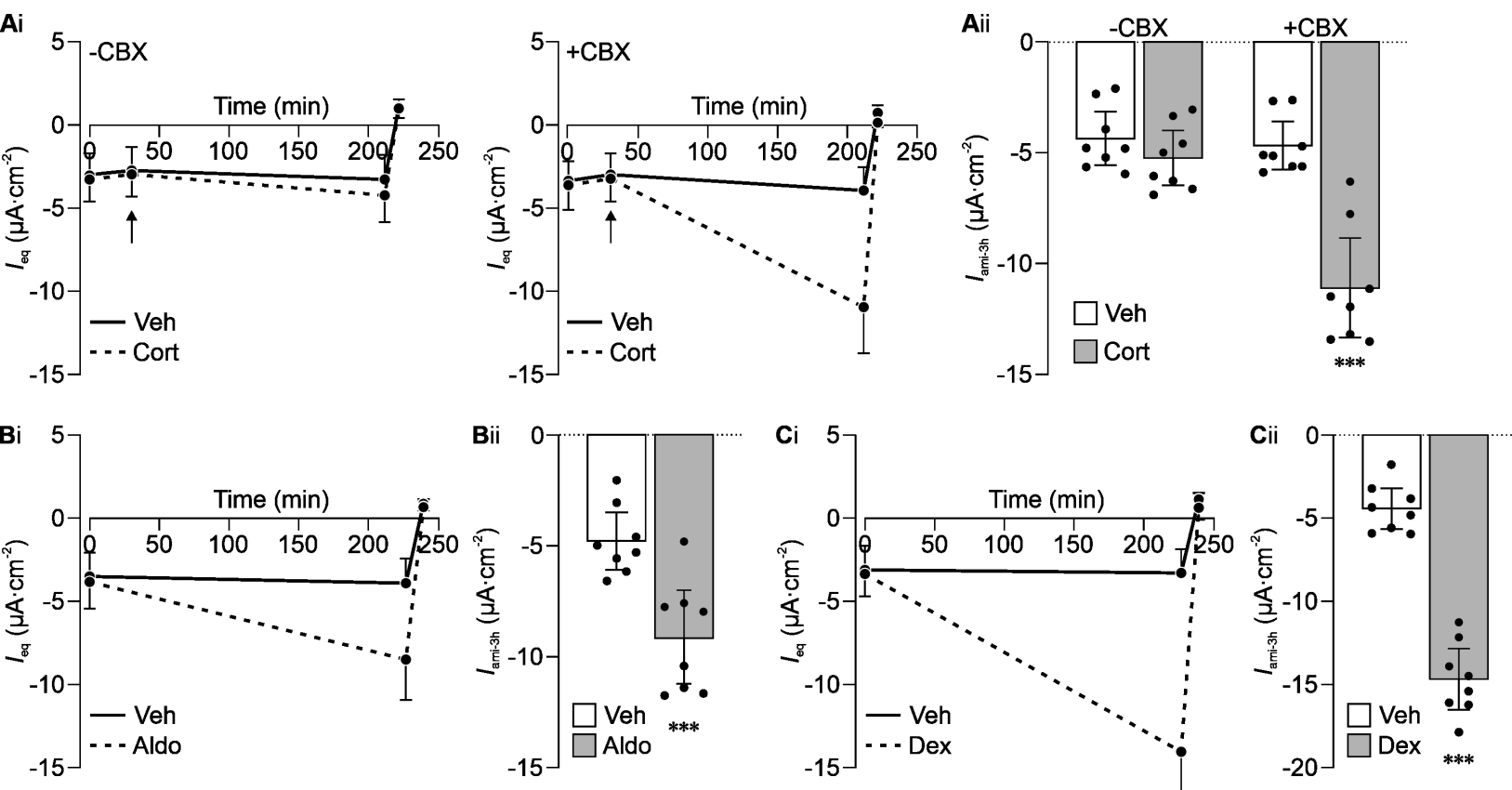


Figure 6

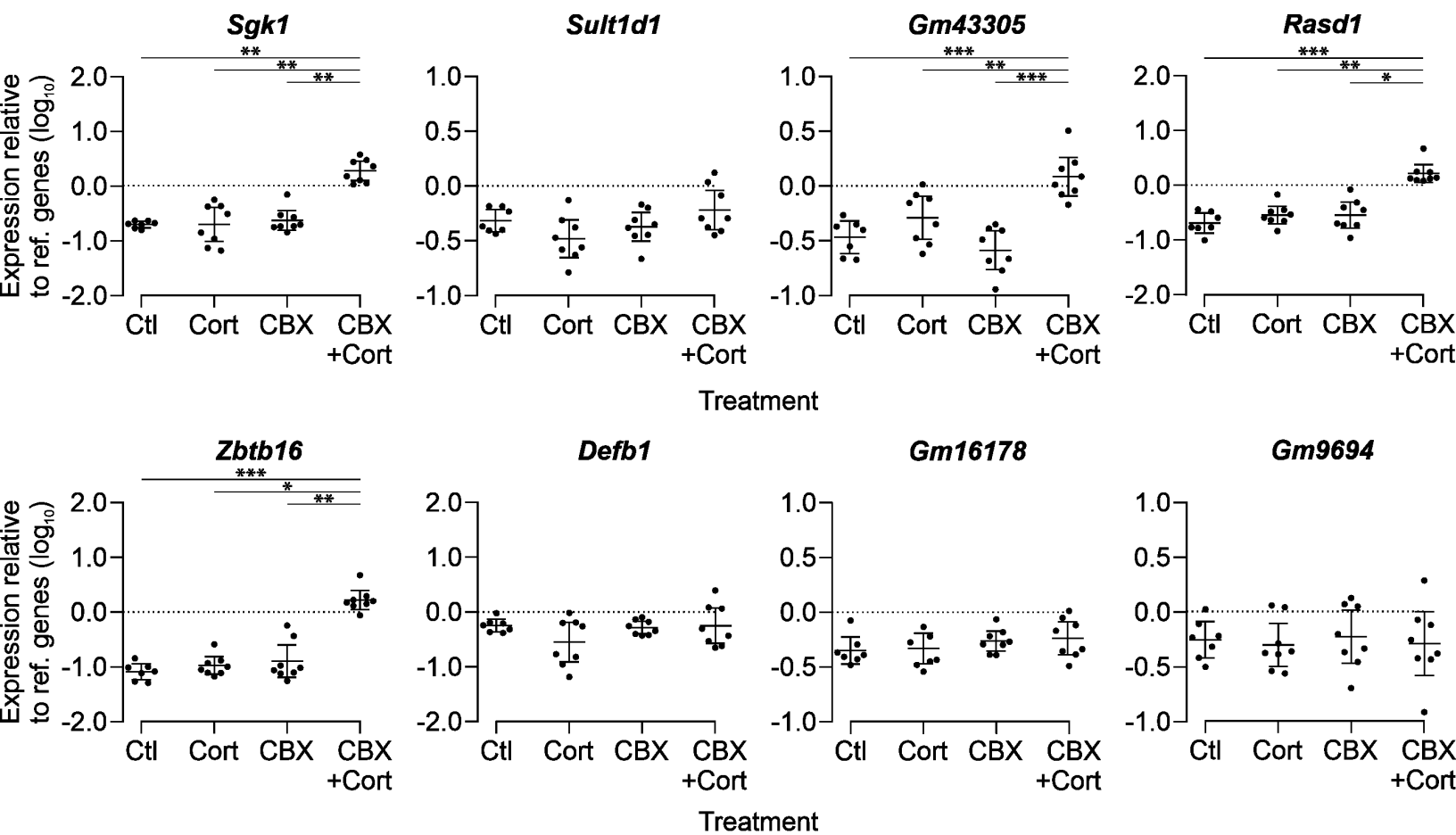


Figure 7

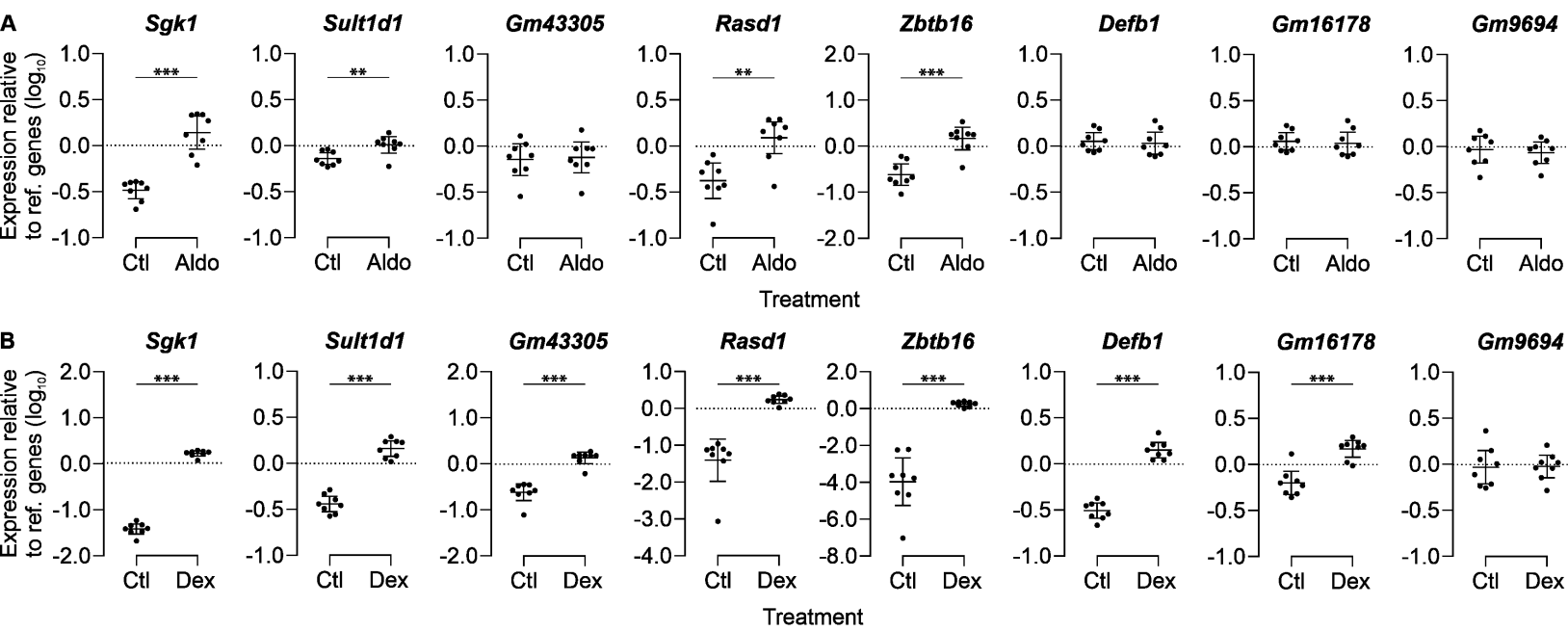


Figure 8

